

**Name of Synchrotron:** 200/500 GeV Synchrotron  
**Institution:** Fermi National Accelerator Laboratory  
**Location:** Batavia, Illinois, 60510  
**Person in Charge:** C.M. Ankenbrandt  
**Data Supplied by:** C.D Moore, T. Yamanouchi  
**Date:** March 1980

**HISTORY AND STATUS**

**Construction Started (date):** December, 1, 1968  
**First Beam Obtained, or Goal (date):** March 1, 1972  
**Total Cost of Facility:** \$ 243 M  
**Funded by:** USAEC  
**Total Accelerator Staff (now):** 313  
**Annual Operating Budget:** \$ 6,15 M (without salaries)  
**Annual Operating Time:** 6222 h  
**“Beam On”:** HE 74% of scheduled time

**ACCELERATOR PARAMETERS***General*

**Accelerated Particles:** Protons  
**Energy:** 200-500 GeV  
**Ring Diam.:** 2000 m  
**Tunnel Sect. (W×H):** 3,05 × 2,44 m

*Injector*

**Type:** 8 GeV Booster  
**Output (Max):** 300 mA at 8 GeV  
**Emittance:** 6,6  $\pi$  mm-mrad (Emittance = Area  $\times \beta\gamma$  at 90% current)  
**Injection Period:** Thirteen 1,6  $\mu$ sec pulses in 0,8 sec.  
**Inflector Type:** Electromagnetic

*Magnet System*

**Focusing Type:** AG  
**Focusing Order:** Q<sub>i</sub>OBBBBQ<sub>d</sub>OBBBB (FODO)  
**Betatron Freq.:**  $\nu_H$ : 19,4;  $\nu_V$ : 19,4  
**No. Magnets:** 774  
**Bending Field:** At inj.: 0,0396 T; at max: 2,229 T  
**No. Quads:** 240  
**Grad.:** At inj.: 0,005396 T/m; at max: 0,3013 T/m  
**No. Short Straight Sect.:** 6  
**No. Long Straight Sect.:** 6  
**Rise Time:** 2,5 s  
**Power Input Peak:** 96 MW  
**Filed index:** Sep. fn  
**Length (ea):** 6,1 m  
**Length (ea):** 2,1 m  
**Length:** 14,589 m  
**Length:** 50,834 m  
**Flat Top Time:** 1 s  
**Mean:** 39,6 MW

*Acceleration System*

**No. Cavities:** 18  
**Harmonic Number:** 1113  
**RF Range:** 52,813 to 53,105 MHz  
**Energy Gain:** 3700 keV/turn  
**Radiation Loss:** 0,0006 keV/turn  
**RF Power Input Peak:** 1800 kW  
**Length (ea):** 1,8 m  
**Mean:** 800 kW

*Vacuum System*

**Material of Vac. Chamber:** Stainless steel  
**Aperture of Vac. Chamber:** 50,8 × 101,6 mm  
**Average Pressure:** 4 × 10<sup>-8</sup> torr  
**Pumps (No., Type, Speed):** 850 triode ion pump, 30 l/s; 37 diode ion pump, 600 l/s

*Extraction System*

**Type:** Resonant with F48 septum  
 Resonant with D0 septum  
 Fast kicker with C48 kicker

**Length of Spill:** 1 ms to 5 s  
 1 ms to 5 s  
 -

*Published Articles Describing Machine*

-

**ACCELERATOR PERFORMANCE**

	<b>Normal (or Goal)</b>	<b>Maximum Achieved</b>
<b>Energy (GeV):</b>	400	500
<b>Resolution <math>\Delta E/E</math> (%):</b>	-	-
<b>Repet. Rate (pulse/s):</b>	1/10	1/8
<b>Pulse Width at Peak E:</b>	1 sec	-
<b>Duty Factor, Macroscopic (%):</b>	86	96
<b>Internal Beam (part/pulse):</b>	$2 \times 10^{13}$	$2,7 \times 10^{13}$
<b>(part/s):</b>	$2 \times 10^{12}$	-
<b>Beam Emittance:</b>	11,7 $\pi$ mm-mrad (Emittance = Area $\times \beta\gamma$ at 90% current)	
<b>Other Data:</b>	-	

**SECONDARY BEAMS**

<b>Particle</b>	<b>Momentum Range</b>	<b>No. of Beams</b>	<b>Other Inform.</b>
Charged hadrons	20-40 geV	8	-
$K^0$	-	-	$2 \times 10^6$ at 200 GeV
n	-	2	-
$e^-$	40-300 GeV/c	1	-
$\nu$	10-300 GeV/c	1 (4 targ. system)	$2 \times 10^6$
$\Sigma^-$	300 GeV/c	1	$1,5 \times 10^6 \mu$ at 225 GeV
u	25-272 GeV/c	1	-
$\gamma$	10-280 GeV/c	2	-

**RESEARCH PROGRAMME**

<b>Total Experimental Areas:</b>	10500 m <sup>2</sup>	
<b>No. Internal Targets:</b>	1	<b>No. Ext. Targets: 9</b>
<b>No. Separated Beams:</b>	0	
<b>No. Beams Served At Same Time:</b>	12 max	
<b>Total Power Used (Average) for Research:</b>	20 MW	
<b>No. User Groups:</b>	135 Total	
<b>Total Research Staff:</b>	106 in house, 744 outside	
<b>Ann. Research Budget:</b>	\$ 1 M (without sal.) in house	
<b>Annual Research Time:</b>	5600 h scheduled	

*Other Relevant Parameters or Notable Features*

-

*Recent Improvement or Modification to Machine*

-

**Name of Synchrotron:** Tevatron  
**Institution:** Fermi National Accelerator Laboratory  
**Location:** Batavia, Illinois, 60510 USA  
**Person in Charge:** - **Date:** April 1980  
**Data Supplied by:** -

**HISTORY AND STATUS**

**Construction Started (date):** -  
**First Beam Obtained, or Goal (date):** -  
**Total Cost of Facility:** -  
**Funded by:** US Department of Energy  
**Total Accelerator Staff (now):** -  
**Annual Operating Budget:** -  
**Annual Operating Time:** -  
**“Beam On”:** -

**ACCELERATOR PARAMETERS***General*

**Accelerated Particles:** Protons  
**Energy:** 800~1000 GeV  
**Ring Diam.:** 2000 m **Tunnel Sect. (W×H):** 3,05 × 2,44 m

*Injector*

**Type:** Main ring (Synchrotron)  
**Output (Max):**  $2,7 \times 10^{13}$ /pulse at 150 GeV  
**Emittance:**  $20 \pi$  mm-mrad (Emittance = Area  $\times \beta\gamma$  at 90% current)  
**Injection Period:** 20  $\mu$ s  
**Inflector Type:** Pulsed magnetic kicker and Lambertson magnet

*Magnet System*

**Focusing Type:** AG sep. fn. **Filed index:** -  
**Focusing Order:** FODO  
**Betatron Freq.:**  $\nu_H$ : 19,40;  $\nu_V$ : 19,40  
**No. Magnets:** 774 **Length (ea):** 6,12 m  
**Bending Field:** At inj.: 0,66 T; at max: 4,42 T  
**No. Quads:** 216 **Length (ea):** 1,68\* m  
**Grad.:** At inj.: 11,4 T/m; at max: 75,9 T/m  
**No. Short Straight Sect.:** 204 **Length:** 2,3 m  
**No. Long Straight Sect.:** 6 **Length:** 53 m  
**Rise Time:** 11~17 s **Flat Top Time:** 1~10 s  
**Power Input Peak:** - **Mean:** -

*Acceleration System*

**No. Cavities:** 6 **Length (ea):** 2,75 m  
**Harmonic Number:** 1113  
**RF Range:** 53 MHz  
**Energy Gain:** 1580 keV/turn  
**Radiation Loss:** -  
**RF Power Input Peak:** - **Mean:** -

*Vacuum System*

**Material of Vac. Chamber:** Stainless steel  
**Aperture of Vac. Chamber:** -  
**Average Pressure:** -  
**Pumps (No., Type, Speed):** Cold Bore 4,6 K

*Extraction System*

**Type:** Slow resonant  $\frac{1}{2}$  integer  
Fast resonant  $\frac{1}{2}$  integer  
**Length of Spill:** 1 – 10 s  
0,1 – 0,3 ms

*Published Articles Describing Machine*

A report on the Design of the Fermi National Accelerator Laboratory Superconducting Accelerator, May 1979  
Fermi National Laboratory

**ACCELERATOR PERFORMANCE**

	<b>Normal (or Goal)</b>	<b>Maximum Achieved</b>
<b>Energy (GeV):</b>	800~1000	-
<b>Resolution <math>\Delta E/E</math> (%):</b>	-	-
<b>Repet. Rate (pulse/s):</b>	-	-
<b>Pulse Width at Peak E:</b>	1 ~ 2 /min	-
<b>Duty Factor, Macroscopic (%):</b>	-	-
<b>Internal Beam (part/pulse):</b>	$>2 \times 10^{13}$	-
<b>(part/s):</b>	-	-
<b>Beam Emittance:</b>	$20 \pi$ mm·mrad (Emittance = Area $\times \beta\gamma$ at 90% current)	
<b>Other Data:</b>	-	

**SECONDARY BEAMS**

<b>Particle</b>	<b>Momentum Range</b>	<b>No. of Beams</b>	<b>Other Inform.</b>
-	-	-	-
-	-	-	-
-	-	-	-
-	-	-	-
-	-	-	-
-	-	-	-
-	-	-	-
-	-	-	-
-	-	-	-

**RESEARCH PROGRAMME**

<b>Total Experimental Areas:</b>	-	<b>No. Ext. Targets:</b>	-
<b>No. Internal Targets:</b>	-		
<b>No. Separated Beams:</b>	-		
<b>No. Beams Served At Same Time:</b>	-		
<b>Total Power Used (Average) for Research:</b>	-		
<b>No. User Groups:</b>	-		
<b>Total Research Staff:</b>	-		
<b>Ann. Research Budget:</b>	-		
<b>Annual Research Time:</b>	-		

*Other Relevant Parameters or Notable Features*

\* 180 normal quadrupoles. There are 36 matching quadrupoles of various length.

*Recent Improvement or Modification to Machine*

-

## THE LATTICE OF THE SPS

*E.J.N. Wilson*

*European Organization for Nuclear Research, CERN, Geneva, Switzerland*

### ABSTRACT

After reviewing many alternatives, the SPS design team selected a FODO separated function lattice for the SPS. Periodicity and Q were chosen bearing in mind cost of construction, space for major accelerator components, extraction and the provision of adequate beam acceptance in spite of the influence of non-linear stop-bands.

### 1. GENERAL DESCRIPTION

The 1964 design study<sup>1</sup> of the 300 GeV machine was based upon a combined function lattice rather similar to that of the 25 GeV CERN PS. The mean radius at a field of 1,2 T was 1200 m. In 1967<sup>2</sup> Fermilab decided to adopt a separated function lattice for their main ring. Simple dipole magnets were designed to operate at 1,8 T and a peak energy of 400 GeV was quoted for a ring only 1000 m in radius.

CERN made a detailed reappraisal<sup>3</sup> of both types of lattice and decided to change to a separate function configuration, not because there was any significant cost saving to be had but because there was a certain flexibility in the separate function design. Space for major accelerator components, such as injection and extraction systems could be provided simply by leaving out bending magnets, this without either interrupting the regular focussing properties of the machine or introducing special matched insertions. Apart from these minor conveniences which tipped the scale in favour of the new lattice, the separate function machine had two attractive features which proved crucial when later approval for the project was sought.

This comparison had shown that all other things being equal separated function machines were more compact. Their window frame bending magnets could operate at a field 50% higher than the gradient magnets of a combined function machine. Even allowing space for the quadrupoles of the separate function machine one saved several hundred metres radius. It was possible to propose a 400 GeV machine which fitted the limited confines of the CERN - Prevezin site, taking advantage of CERN's existing infrastructure and resolving the site selection controversy.

The other advantage of the separate function principle was that construction could start with the modest intention of filling half of the space in each cell with bending magnets and later, once the major component costs and construction schedules became clear one might exercise the option to install the missing magnets bringing the energy to 400 GeV.

The only disadvantage for the separate function lattice, which became apparent during running-in, is the need for very careful regulation of the two quadrupole and dipole circuits, but this difficulty has been overcome and is by far outweighed by the freedom to move the Q values at will.

The similarity between the SPS and its elder sister in Batavia is no accident. Many alternatives were studied, but, given similar boundary conditions it was not unnatural to arrive at a similar optimum.

### 2. APERTURE REQUIREMENTS

The SPS was the first CERN machine to rely on closed orbit correction to achieve the full acceptance needed for the design intensity. It was thought, that with careful magnet design, remanent and stray field orbit distortions would be smaller than about 30 mm horizontally, and could be corrected at injection with a small dipole at each quadrupole. Provided the alignment errors could be kept within tolerance met at the ISR, distortions present at high field would be less than 15 mm and be corrected by moving a few selected quadrupoles.

Having used this procedure to arrive at magnet apertures the SPS designers checked that there was sufficient horizontal aperture for the resonant growth of slow extraction needed to reduce losses at the septum and pondered whether magnet pole edges and coil were far enough from the beam to ensure the field tolerances necessary to avoid betatron resonances in a large accelerator. An extra 10 mm was added to the horizontal aperture, a measure which in retrospect seems to have had a beneficial effect at very little extra cost. Fig. 1 shows how apertures were finally defined<sup>4</sup>.

Measurements of closed orbit without correction lie within these predictions and correction procedures are even more effective than had been hoped.

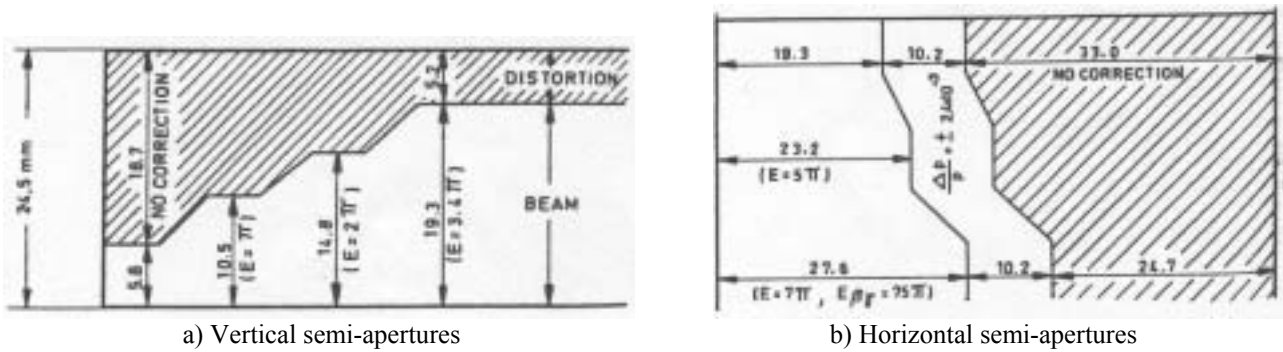


Fig. 1 Breakdown of SPS injection apertures

### 3. PARAMETERS OF A NORMAL PERIOD

A FODO configuration was chosen because of its simplicity, because the beta values at the quadrupoles are very different, an important consideration if one wants correction magnets to act orthogonally, and because the fraction of the circumference devoted to quadrupoles is smaller than in other configurations.

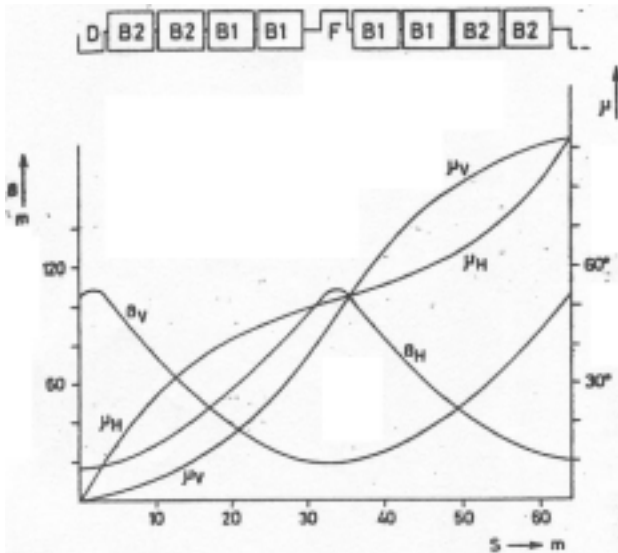


Fig. 2 Lattice functions

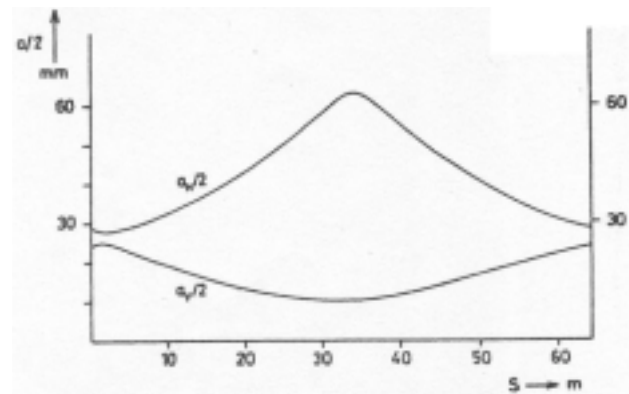


Fig. 3 Beam envelope fitting mechanical apertures

Fig. 2 shows the lattice functions. After a careful cost optimisations which included coefficients for magnet aperture, stored energy of the power supply, tunnel circumference and running costs, a periodicity of 108 and a phase advance of  $92^\circ$  per period were chosen. Lattices with fewer periods and lower Q tended to have large lattice functions and apertures. Those with larger number of periods required more focussing and bending magnets. The many factors of 108 left several option open in the symmetrical arrangement of correction magnets and a phase advance of almost  $90^\circ$  was a considerable conceptual simplification.

Un retrospect the rather high Q had another advantage, it tended to reduce  $\alpha_p$  which has a direct influence on the chromaticity Q spread caused by sextupole guide field imperfections.

Fig. 3 shows the envelope of a beam which just fits the mechanical apertures. The cost saving to be had from matching two types of dipole apertures to the envelope outweighed the extra tooling and development costs.

On the other hand although the beam has a very different aspect ratio at F and D quadrupoles both sections fit well into a single symmetrical quadrupole design. Of course the F and D quadrupoles are powered by independent power supplies to allow Q tuning but are otherwise identical.

### 4. LONG STRAIGHT SECTION INSERTIONS

The machine is divided into six identical super-periods. Each super-period is composed of fourteen normal periods and a sequence of four special periods which form the long straight section insertion. Bending magnets are omitted from the special periods to make room for the more bulky components of the machine but the regular spacing of quadrupoles is preserved throughout the super-period.

The sequence of special periods in the insertion is shown in Fig. 4. The pattern is mainly determined by the design of the extraction channel.

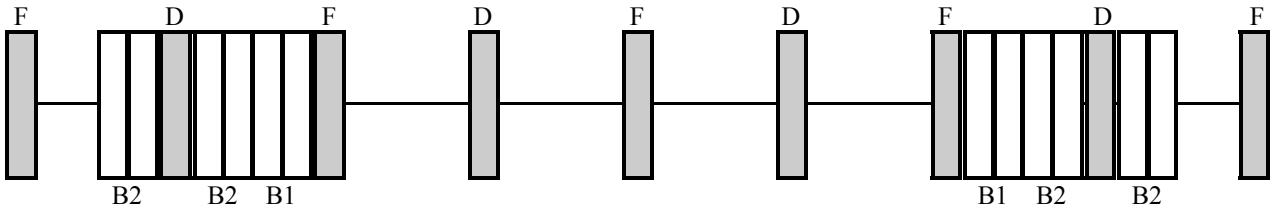


Fig. 4 Long straight section insertion

The six long straight sections of the machine are equally spaced around the ring. Straight section number 1 is assigned to the injection system for the input beam from the CPS, the second to an extraction system to the North Experimental Area, a third to the RF accelerating system, a fourth to a beam dump and the fifth reserved for future developments. Straight section 6 is used for the extraction system to the West Hall.

No special measures were taken to reduce the beat of the momentum compaction function Fig. 5. It is a convenience to have rather small  $\alpha_p$  in the long straight sections.

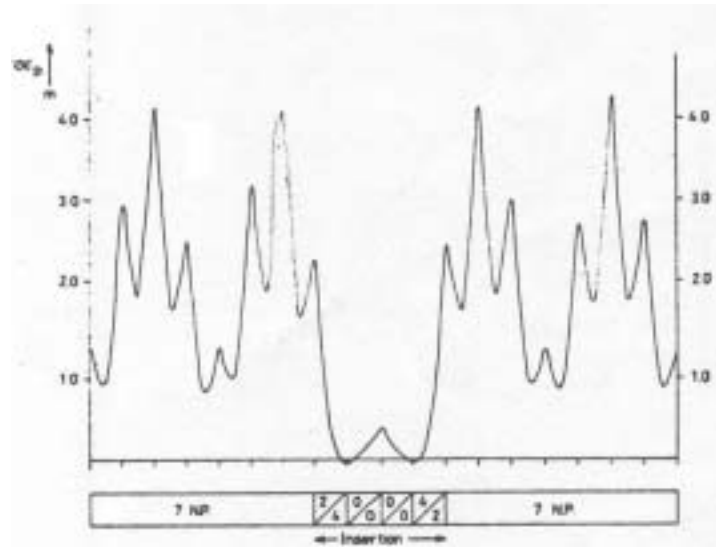


Fig. 5 Momentum compaction function in one super-period

As the design progressed it was decided to enlarge the four central quadrupoles in the three symmetrically spaced straight sections for extraction and beam dumping. By scaling both length and aperture by the same ratio 11:9, no first order perturbation is made to the dynamics and the larger quadrupoles have space between their coils for the emerging extracted beam.

### 5. CHOICE OF WORKING POINT

One of the advantages of the separate function machine is that one has the freedom to explore various Q values with the beam. Nevertheless certain elementary precautions must be taken and a nominal Q value must be chosen as a basis for the specification of other components.

Fig. 6 shows the numerology of systematic sum resonances generated by multiples of 6, the superperiodicity of the SPS. The spacing of these lines becomes closer the smaller the superperiodicity but for  $s=6$  none fall within half integer squares. At the extremities of the diagram where Q is a multiple of s the momentum compaction function beats violently. A nominal Q value just above 27,5 was chosen remembering that the flexibility could be exploited to change Q if necessary.

In addition to the structure resonances there are of course the more numerous but weaker stopbands driven by random multipole errors and which have the same pattern in each integer square. It seems prudent to have a small Q split to

avoid the diagonal coupling resonance  $Q_H = Q_V$  and preferable to be close to the half integer rather than the integer where closed orbit magnification factors become large, thus arriving at  $Q_H = 27,6$ ,  $Q_V = 27,55$ .

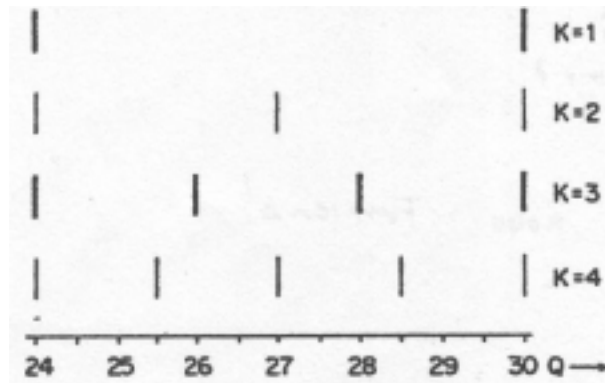


Fig. 6 Numerology of structure resonances

During construction Fermilab found empirically that fifth order structure resonances, contrary to widely held beliefs, are destructive to a beam when synchrotron motion or magnet ripple causes repetitive crossing. It therefore was no surprise to find that it was better to work the SPS at 27,4 rather than the nominal 27,6 which is a fifth order structure resonance.

## 6. RUNNING-IN EXPERIENCE

In general the design calculations of beam sizes and orbit distortions for the SPS have proved valid and the lattice has no unexpected vices. Designers of other machine components have managed to fit into the straight sections available – there is even room to augment some systems. The separated function principle and the flexibility it gives in choice of Q has already proved its worth in avoiding one of the unexpected pitfalls of an extrapolation in accelerator design of factor 10. Some pointers to how one might approach the design of an even larger ring emerge rather clearly.

- i) Steering the first turn and correcting closed orbit distortion to a few millimetres can be assumed from the first days of running-in.
- ii) The control of the chromatic Q spread with sextupoles is both essential and not very difficult in a machine of this size. The high Q of the SPS is an advantage in this respect.
- iii) The SPS though constructed to very fine tolerances must be tuned carefully if beam loss due to non-linear resonances is to be avoided. Future machine designing would do well to weigh this fact strongly in their lattice optimisation and choice of aperture.
- iv) Fifth and higher order stopbands are not stable when crossed repetitively.

\* \* \*

## REFERENCES

1. CERN 300 GeV Design Study, CERN/563 (1964).
2. Design Report, national Accelerator Laboratory, FNAL (1968).
3. J.B. Adams, E.J.N. Wilson, Nuc. Inst. Meth., 87 (1970), p.157.
4. The 300 GeV Programme, CERN/1050 (1972).

### HIGH-ENERGY COLLIDER PARAMETERS: ep, $\overline{pp}$ , and pp Colliders

The number here were received from representatives of the colliders in late 1999. Many of the numbers of course change with time, and only the latest values (or estimates) are given here. Quantities are, where appropriate, r.m.s. H, V and s.c. indicate horizontal and vertical directions, and superconducting. The SSC is kept for purposes of comparison.

	HERA (DESY)	$\overline{Sp\overline{pS}}$ (CERN)	TEVATRON (Fermilab)	LHC (CERN)		SSC (USA)
Physics start date	1992	1981	1987	2005		Terminated
Physics end date	-	1990	-	-		-
Particles collided	ep	$\overline{pp}$	$\overline{pp}$	pp	PbPb	Pp
Maximum beam energy (TeV)	e: 0,030 p: 0,92	0,315 (0,45 in pulsed mode)	1,0	7,0	2,76 TeV/u	20
Luminosity ( $10^{30} \text{ cm}^{-2}\text{s}^{-1}$ )	14	6	210	$1,0 \cdot 10^4$	0,002	1000
Time between collision ( $\mu\text{s}$ )	0,096	3,8	0,396	0,025	0,125	0,016678
Crossing angle ( $\mu\text{rad}$ )	0	0	0	$\geq 200$	$\leq 200$	100 to 200 (135 nominal)
Energy spread (units $10^{-3}$ )	e: 0,91 p: 0,2	0,35	0,09	0,1	0,1	0,055
Bunch length (cm)	e: 0,83 p: 8,5	20	38	7,5	7,5	6,0
Beam radius ( $10^{-6} \text{ m}$ )	e: 280 (H), 50 (V) p: 265 (H), 50 (V)	$\overline{p}$ : 73 (H), 36 (V) $\overline{p}$ : 55(H), 27 (V)	$\overline{p}$ : 34 $\overline{p}$ : 29	16	15	4,8
Free space at interaction point (m)	$\pm 5,8$	16	$\pm 6,5$	38	38	$\pm 20$
Luminosity lifetime (hr)	10	15	7-30	10	6,7	$\sim 24$
Filling time (min)	e: 60 p: 120	0,5	30	6	20	72
Accelerated period (s)	e: 200 p: 1500	10	86	1200		1500
Injection energy (TeV)	e: 0,012 p: 0,040	0,026	0,15	0,450	177,4 GeV/u	2
Transverse emittance ( $10^{-9} \pi \text{ rad}\cdot\text{m}$ )	e: 42 (H), 6 (V) p: 5 (H), 5 (V)	$\overline{p}$ : 9 $\overline{p}$ : 5	$\overline{p}$ : 3,5 $\overline{p}$ : 2,5	0,5	0,5	0,047
$\beta^*$ , amplitude function at interaction point	e: 1 (H), 0,7 (V) p: 7 (H), 0,5 (V)	0,6 (H) 0,15 (V)	0,35	0,5	0,5	0,5
Beam-beam tune shift per crossing (units $10^{-4}$ )	e: 190(H), 360(V) p: 12 (H), 9 (V)	50	$\overline{p}$ : 38 $\overline{p}$ : 97	34	-	8 head on 13 long range
RF frequency (MHz)	e: 499,7 p: 208,2/52,05	100+200	53	400,8	400,8	359,75
Particles per bunch (units $10^{10}$ )	e: 3 p: 7	$\overline{p}$ : 15 $\overline{p}$ : 8	$\overline{p}$ : 27 $\overline{p}$ : 7,5	10,5	0,0094	0,8
Bunches per ring per species	e: 189 p: 180	6	36	2835	608	17,424
Average beam current per species (mA)	e: 40 p: 90	$\overline{p}$ : 6 $\overline{p}$ : 3	$\overline{p}$ : 81 $\overline{p}$ : 22	536	7,8	71

Circumference (km)	6,336	6,911	6,28	26,659		87,12
Interaction regions	ep: 2; e,p: 1 each, internal fixed target	2	2 high $L$	2 high $L$ +1	1	4
Utility insertions	4	-	4	4		2
Magnetic length of dipole (m)	e: 9,185 p: 8,82	6,26	6,12	14,3		Mostly 14,928
Length of standard cell (m)	e: 23,5 p: 47	64	59,5	106,90		180
Phase advance per cell (deg)	e: 60 p: 90	90	67,8	90		90
Dipoles in ring	e: 396 p: 416	744	744	1232 main dipoles		(H: 8336, V: 88) in 2 rings
Quadrupoles in ring	e: 580 p: 280	232	216	692 focussing +96 skew		2084 in 2 rings
Magnet type	e: C-shaped p: s.c., collared, cold iron	H type with bent-up coil ends	s.c. $\cos\theta$ warm iron	s.c. 2 in 1 cold iron		s.c. $\cos\theta$ cold iron
Peak magnetic field	e: 0,274 p: 4,65	1,4 (2 in pulsed mode)	4,4	8,3		6,790
$\bar{p}$ source accum. rate ( $\text{hr}^{-1}$ )	-	$6 \times 10^{10}$	$20 \times 10^{10}$	-		-
Max. no. $\bar{p}$ in accum. ring.	-	$1,2 \times 10^{12}$	$2,6 \times 10^{12}$	-		-

### HIGH-ENERGY COLLIDER PARAMETERS: $e^+e^-$ Colliders

The number here were received from representatives of the colliders in late 1999. Many of the numbers of course change with time, and only the latest values (or estimates) are given here. Quantities are, where appropriate, r.m.s. H, V and s.c. indicate horizontal and vertical directions, and superconducting.

	CESR (Cornell)	KEKB (KEK)	PEP-II (SLAC)	SLC (SLAC)	LEP (CERN)
Physics start date	1979	1999	1999	1989	1989
Maximum beam energy (GeV)	6	$e^- \times e^+$ : $8 \times 3,5$	$e^-$ : 7-12 (9,0 nom) $e^+$ 2,5-4 (3,1 nom) (nominal $E_{cm}$ : 10,5 GeV)	50	101 in 1999 (105 max foreseen)
Luminosity ( $10^{30} \text{ cm}^{-2}\text{s}^{-1}$ )	830 at 5,3 GeV	10000	3000	2,5	24 at $Z^0$ 100 at $> 90$ GeV
Time between collision ( $\mu\text{s}$ )	0,014 to 0,22	0,002	0,0042	8300	22
Crossing angle ( $\mu\text{rad}$ )	$\pm 2000$	$\pm 11,00$	0	0	0
Energy spread (units $10^{-3}$ )	0,6 at 5,3 GeV	0,7	$e^-/e^+$ : 0,61/0,77	1,2	0,7 $\rightarrow$ 1,5
Bunch length (cm)	1,8	0,4	$e^-/e^+$ : 1,1/1,0	0,1	1,0
Beam radius ( $\mu\text{m}$ )	H: 500 V: 10	H: 77 V: 1,9	H: 157 V: 4,7	H: 1,5 V: 0,5	H: 200 $\rightarrow$ 300 V: 2,5 $\rightarrow$ 8
Free space at interaction point (m)	$\pm 2,2$ ( $\pm 0,6$ to REC quads)	+ 0,75/- 0,58 (+300/-500) mrad cone	$\pm 0,2$ , $\pm 300$ mrad cone	$\pm 2,8$	$\pm 3,5$
Luminosity lifetime (hr)	2-3	2	2,5	-	20 at $Z^0$ 10 at $> 90$ GeV
Filling time (min)	10 (topping up)	8 (topping up)	3 (topping up)	-	20 to setup 20 to accumulate
Acceleration period (s)	-	-	-	-	600
Injection energy (GeV)	6	$e^-/e^+$ : 8/3,5	2,5-12	45,64	22
Transverse emittance ( $\pi$ rad-nm)	H: 240 V: 6	H: 18 V: 0,36	$e^-$ : 48 (H), 1,5 (V) $e^+$ : 48 (H), 1,5 (V)	H: 0,5 V: 0,05	H: 20-45 V: 0,25 $\rightarrow$ 1
$\beta^*$ , amplitude function at interaction point (m)	H: 1,0 V: 0,018	H: 0,33 V: 0,01	$e^-$ : 0,50 (H), 0,015 (V) $e^+$ : 0,50 (H), 0,015 (V)	H: 0,0025 V: 0,0015	H: 1,5 V: 0,05
Beam-beam tune shift per crossing (units $10^{-4}$ )	480	H: 390 V: 520	300	-	830
RF frequency (MHz)	500	508,887	476	-	352,2
Particles per bunch (units $10^{10}$ )	1,15	$e^-/e^+$ : 1,3/3,2	$e^-/e^+$ : 2,1/5,9	4,0	45 in collision 60 in single beam
Bunches per ring per species	9 trains of 4 bunches	5120 (5-10% gap is necessary)	1658	1	4 trains of 1 or 2
Average beam current per species (mA)	260	$e^-/e^+$ : 1100/2600	$e^-/e^+$ : 750/2161	0,0008	4 at $Z^0$ 4 $\rightarrow$ 6 at $>90$ GeV
Beam polarization (%)	-	-	-	$e^-$ : 80	55 at 45 GeV 5 at 61 GeV

Circumference or length (km)	0.768	3.016	2.2	1.45 + 1.47	26.66
Interaction regions	1	1	1 (2 possible)	1	4
Utility insertions	3	3 per ring	5	-	4
Magnetic length of dipole (m)	1.6-6.6	$e^-/e^+$ : 5.86/0.915	$e^-/e^+$ : 5.4/0.45	2.5	11.66/pair
Length of standard cell (m)	16	$e^-/e^+$ : 75.7/76.1	15.2	5.2	79
Phase advance per cell (deg)	45-90 (no standard cell)	450	$e^-/e^+$ : 60/90	108	102/90
Dipoles in ring	86	$e^-/e^+$ : 116/112	$e^-/e^+$ : 192/192	460+440	3280+24 inj. +64 weak
Quadrupoles in ring	104	$e^-/e^+$ : 452/452	$e^-/e^+$ : 290/326	-	520+288 + 8 s.c.
Peak magnetic field (T)	(0.3 normal 0.8 high field) at 8 GeV	$e^-/e^+$ : 0.25/0.72	$e^-/e^+$ : 0.18/0.75	0.597	0.135

	VEPP-2M (Novosibirsk)	VEPP-2000* (Novosibirsk)	VEPP-4M (Novosibirsk)	BEPC (China)	DAΦNE (Frascati)
Physics start date	1974	2001	1994	1989	1999
Maximum beam energy (GeV)	0.7	1.0	6	2.2	0.510 (0.75 max.)
Luminosity ( $10^{30} \text{ cm}^{-2}\text{s}^{-1}$ )	5	100	50	10 at 2 GeV 5 at 1.55 GeV	5 ( $\rightarrow$ 50)
Time between collision ( $\mu\text{s}$ )	0.03	0.04	0.6	0.8	0.0027 – 0.0108
Crossing angle ( $\mu\text{rad}$ )	0	0	0	0	$\pm(1.0 \text{ to } 1.5)\times 10^{-4}$
Energy spread (units $10^{-3}$ )	0.36	0.64	1	0.58 at 2.2 GeV	0.40
Bunch length (cm)	3	4	5	$\approx 5$	2 ( $\rightarrow$ 3)
Beam radius ( $10^{-6} \text{ m}$ )	H: 300 V: 10	125 (round)	H: 1000 V: 30	H: 890 V: 37	H: 2100 V: 21
Free space at interaction point (m)	$\pm 1$	$\pm 1$	$\pm 2$	$\pm 2.15$	$\pm 0.46$ ( $\pm 157 \text{ mrad cone}$ )
Luminosity lifetime (hr)	continuous	continuous	2	7 - 12	1 ( $\rightarrow$ 2)
Filling time (min)	continuous	continuous	15	30	2 (per beam)
Acceleration period (s)	-	-	150	120	-
Injection energy (GeV)	0.2 – 0.6	0.2 – 1.0	1.8	1.55	0.510
Transverse emittance ( $10^{-9} \pi \text{ rad}\cdot\text{m}$ )	H: 110 V: 1.3	H: 250 V: 250	H: 400 V: 20	H: 660 V: 28	H: 1000 V: 10
$\beta^*$ , amplitude function at interaction point (m)	H: 0.45 V: 0.045	H: 0.06 V: 0.06	H: 0.75 V: 0.05	H: 1.2 V: 0.05	H: 4.5 V: 0.045
Beam-beam tune shift per crossing (units $10^{-4}$ )	H: 200 V: 500	H: 750 V: 750	500	350	400
RF frequency (MHz)	200	172	180	199.53	368.25
Particles per bunch (units $10^{10}$ )	2	16	15	20 at 2 GeV 22 at 1.55 GeV	3 ( $\rightarrow$ 9)
Bunches per ring per species	1	1	2	1	30 - 120
Average beam current per species (mA)	50	300	80	40 at 2 GeV 22 at 1.55 GeV	800 ( $\rightarrow$ 1500)
Circumference or length (km)	0.018	0.024	0.366	0.2404	0.0977
Interaction regions	2	2	1	2	1 ( $\rightarrow$ 2)
Utility insertions	1	2	1	4	2 $\times$ 2
Magnetic length of dipole (m)	1	1.2	2	1.6	$e^+$ : 1.21/0.99 $e^-$ : 1.21/0.99
Length of standard cell (m)	4.5	12	7.2	6.6	-
Phase advance per cell (deg)	280	H: 738 V: 378	65	$\approx 60$	-
Dipoles in ring	8	8	78	40 + 4 weak	$e^+$ : 8(+4 wigglers) $e^-$ : 8(+4 wigglers)

Quadrupoles in ring	20	20	150	68	e <sup>+</sup> /e <sup>-</sup> : 53/53
Peak magnetic field (T)	1.8	2.4	0.6	0.9028 at 2.8 GeV	1.2 (→1.76) dipoles 1.8 wigglers

\*VEPP-2000 is a major upgrade of VEPP-2M

## THE DESIGN OF THE WNR PROTON STORAGE RING LATTICE

*R.K. Cooper and G.P. Lawrence*

*University of California*

*Los Alamos Scientific Laboratory, P.O. Box 1663, Los Alamos, New Mexico, 87545*

### 1. INTRODUCTION

The Weapons Neutron research Facility, now approaching operational status, is a pulsed neutron time-of-flight facility utilizing bursts of 800 MeV protons from the LAMPF linac. The protons strike a heavy metal target and produce a broad energy spectrum of neutrons via spallation reactions. Ideally the width of the proton pulse should approach a delta function in order to achieve good neutron energy resolution. Practically, the shortest pulse that can be employed in the facility is that produced by a single LAMPF micropulse, which, at design current, contains approximately  $5 \times 10^8$  protons. With the addition of a storage ring capable of accumulating many micropulses, this intensity can be increased, as can the repetition rate. Moreover, by storing an unbunched beam, a low repetition rate, very intense proton burst can be generated. This latter mode of usage allows neutron time-of-flight studies using large neutron targets, for which pulse lengths of the order of several hundreds nanoseconds are suitable. The primary goals of the ring reported on here are: (i) to increase the intensity of the burst to  $10^{11}$  protons while retaining a short pulse length; (ii) to increase the repetition rate of the bursts by at least a factor of six; and, (iii) to store as many particles as possible, uniformly distributed around the ring

### 2. OPERATIONAL CHARACTERISTICS

In the mode of operation in which short pulses are accumulated for time-of-flight use, the ring will be filled 120 times per second and will essentially superpose [in six dimensional phase space, employing charge exchange (stripping) injection] 200 LAMPF micropulses<sup>1,2</sup>. the LAMPF H<sup>-</sup> pulse structure will be modified for ring injection purpose so that micropulses will be separated by 50 ns instead of the usual 5 ns (during that portion of the LAMPF pulse for which the ring is not being filled, i.e., 440  $\mu$ s out of 500  $\mu$ s, the pulse structure will be unchanged). Since the circulation time of the ring is 300 ns, it will contain six circulating bunches, each of which will be separately extracted during the 7.8 ms between filling periods. Thus the pulse repetition frequency of the facility will be increased by a factor six, while the pulse intensity will be increased by a factor of 200.

In the high current mode of operation, it is expected that the ring will be filled (again employing charge exchange injection) with one or more full LAMPF macropulses ( $5 \times 10^{13}$  protons/macropulse). Each macropulse requires that the beam emittance be greater than  $1.36 \pi \times 10^{-5}$  m-rad to contain this current. The repetition rate for this mode is limited by the existing shield at the WNR target which permits 1-2% of LAMPF design intensity to be used.

### 3. THE DESIGN

The ring lattice was chosen to have a separated function for tune flexibility and simplicity of construction. In order to avoid the negative mass instability for the high current mode it was decided to operate the ring below transition; the particle  $\gamma$  is 1.85, so a design transition gamma of approximately 2 was chosen. This figure in turn indicates that a nominal radial tune,  $\nu_x$ , of 2.25 would be desirable.

The circumference of the ring was chosen to be compatible with a maximum pulse length generated by single turn extraction of approximately 250 ns. A number of straight sections appropriate to injection, extraction and beam manipulation, including the possibility of future development of a second extraction section were deemed required. With a tune of 2.25 and a betatron phase advance of approximately  $\pi/2$  per period to minimize the betatron functions, an eight-sided figure seemed indicated. An octagonal lattice was in fact chosen to allow placing the injection and extraction functions in separate straight sections within the constraint that the ring must be supplied from and return particles to the WNR beam line. Figure 1 shows the component layout of the ring lattice, while Table 1 summarizes the lattice parameters and Table 2 the ring operating characteristics. Figure 2 is a plot of the square root of the radial and vertical betatron functions as well as the off momentum function  $\eta = \Delta r/(\Delta p/p)$ .

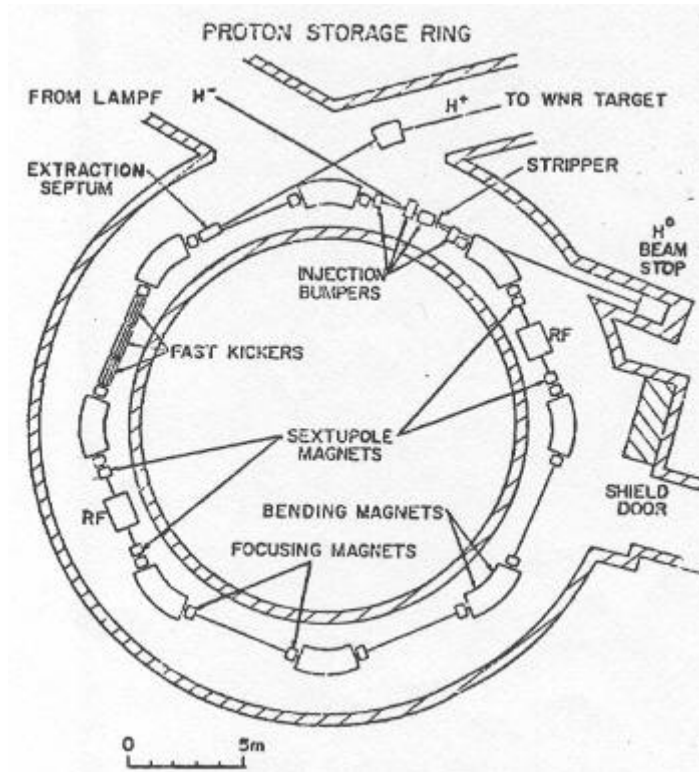


Fig. 1. Plan View of the Ring

Circumference	75,240 m
Mean Radius	11,975 m
Orbit Radius in bending magnets	4,881 m
Length of bending magnets	3,834 m
Gap height	0,080 m
Gap width (useful field)	0,12 m
Length of quadrupole magnets	0,400 m
Bore of quadrupole magnets	0,11 m
Length of straight section	4,171 m

Table 1. Ring Dimensions

Betatron Oscillations per revolution (nominal)	
Radial, $\nu_x$	2.25
Vertical, $\nu_y$	2.25
Transition gamma, $\gamma_t$	2.07
Bending magnet field strength	1.000 T
Focusing quadrupole gradient	3.116 T/m
Defocusing quadrupole magnet	-3.980 T/m
Bunched operation	
No. of bunches	6
Length of bunch	1 ns
RF frequency	603.75 MHz
Harmonic number	180
Space charge limit for $\epsilon_x = \epsilon_y = \pi \times 10^{-5}$ m-rad ( $\Delta v = 0.2$ )	$1.23 \times 10^{11}$ p/bunch
Unbunched operation	
Space charge limit for $\epsilon_x = \epsilon_y = \pi \times 10^{-5}$ m-rad	$3.69 \times 10^{13}$
Chromaticity $\partial\nu/\partial(\Delta p/p)$	
Radial	-0.30
Vertical	-0.33

Table 2. Operating Characteristics

Injection is accomplished through a set of pulsed magnets which bring the circulating proton beam and the incoming H<sup>-</sup> beam into spatial coincidence at the location of the stripper foil. The magnets are pulsed in order to increase foil lifetime and to control emittance growth effects due to scattering in the foil<sup>3</sup>. A calculation of the space charge limit for the bunched mode of operation for the given lattice shows that the (unnormalized) emittance of the stored beam must be greater than  $0.8 \pi \times 10^{-5}$  m-rad (both planes); since the emittance of the LAMPF linac is approximately  $0.1 \times 10^{-5}$  m-rad, the emittance must be degraded by injecting off the equilibrium orbit.

The rf system to maintain the bunch length of the accumulated micropulses must provide somewhat larger buckets than those in the LAMPF accelerator, due to the fact that the micropulses spread in length in the beam transport system. For a LAMPF  $\Delta p/p$  of 0.002 (FWHM), a 450 kV, 603.75 MHz rf bunching system will maintain a 1ns bunch<sup>4</sup>. This rf voltage may be applied in one or more of the straight sections. Additional rf may be required for synchrotron frequency splitting<sup>5</sup>, or for bunching on the first harmonic to minimize spill during single turn extraction.

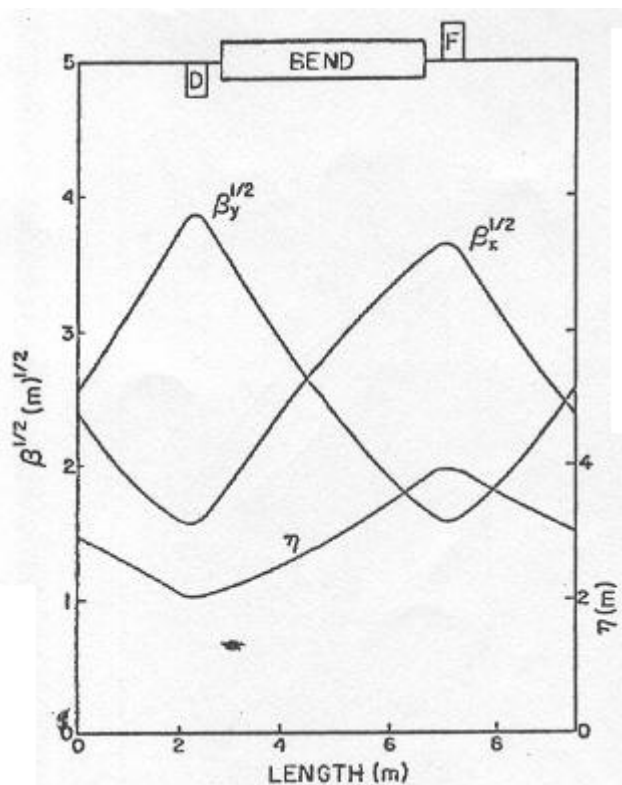


Fig. 2. Beta Functions and Off-Momentum Orbit

The bunches are separately extracted by a set of fast kicker magnets of the parallel plate transmission line type. These kickers must perform their function within 100 ns (twice the time between bunches) and with a 720 Hz repetition rate. These parameters represent the state of the art; further improvements would enhance the capabilities of the WNR facility as a pulsed neutron source. The kickers give an overall kick of 6 mrad; the beam then receives a further kick from the defocusing quadrupole magnet. Upon leaving the following focusing quadrupole, the beam is headed toward the equilibrium orbit but is intercepted by the extraction septum magnet. Figure 3 shows the details of the extraction orbit.

#### 4. CALCULATIONS

A summer study which used a reference lattice similar to that reported on here was held in Los Alamos in August, 1976. The rf bunching requirements were examined, the extraction system was studied, and various instability growth times were calculated. No serious obstacle to successful operation of the ring was discovered. The results of the summer study are summarized in the report cited in Ref. 4.

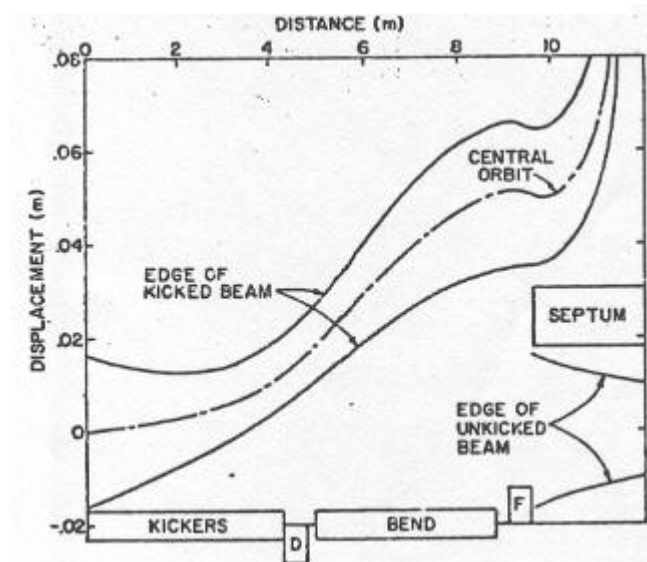


Fig. 3. Extraction Orbit Details

\* \* \*

#### ACKNOWLEDGMENT

The authors wish to tanks Drs. A. Garren and M. Foss for helpful discussion and criticism.

#### REFERENCES

1. J. Simpson, "Operating Results from the ANL Booster", IEEE Trans. On Nucl. Science NS-20, pp 198-201 (1973).
2. A. Kaminsky, R. Meshcherov and M. Popova, "Efficiency of Charge Exchange Injection in Proton Accelerators and Storage Rings", Nucl. Inst. And Meth. 137, pp. 183-188 (1976).
3. R. Cooper and G. Lawrence, "Beam Emittance Growth in a Proton Storage Ring Employing Charge Exchange Injection", IEEE Trans. On Nucl. Science NS-22, pp 1916-1918 (1975).
4. L. Smith, in "Proton Storage Ring Summer Workshop Contributions", LA-6749-C (in preparation), Los Alamos Scientific Laboratory.
5. M. Allen, M. Lee and P. Morton, "Synchrotron Frequency Splitting in the SLAC Storage", IEEE Trans. On Nucl. Science NS-18, 1084-1085 (1971).

**Name of Machine:** Clinton P. Anderson Meson Physics Facility (LAMPF)  
**Institution:** Los Alamos Scientific Laboratory  
**Location:** Los Alamos, New Mexico, USA  
**Person in Charge:** L. Rosen **Date:** March 1980  
**Data Supplied by:** D. Hagerman

**HISTORY AND STATUS**

**Construction Started (date):** 1968  
**First Beam Obtained, or Goal (date):** June, 1972  
**Total Cost of Facility:** \$ 57 M  
**Funded by:** U.S. Department of Energy  
**Total Accelerator Staff (now):** 100  
**Annual Operating Budget:** -  
**Annual Operating Time:** 4500 h (1979)  
**“Beam On”:** 80% of scheduled time

**ACCELERATOR PARAMETERS***Physical Dimensions*

**Accelerator Length:** 785 m **Diam:** -  
**Tunnel Size (L×H×W):** 900 × 4 × 4

*Injection System*

**Ion Source:** Duoplasmatron  
**Output :** 30 mA **Emittance:** -  
**Injector Type:** Cockcroft-Walton (3)  
**Output:** 25 mA **Emittance:** -  
**Buncher:** Double-drift, Single-frequency

**ACCELERATION SYSTEM**

	I	II
<b>Type (Linac):</b>	Drift Tube	Side-Coupled Cavity
<b>Beam Energy (MeV):</b>	0.75-100	100-800
<b>Total Length (m):</b>	63	727
<b>Energy Gain (MeV/m):</b>	1-1.9	1.1
<b>RF Freq. (MHz):</b>	201.25	805
<b>Field Mode:</b>	TM010	TM010
<b>Q (× 10<sup>3</sup>):</b>	60-75	18-25
<b>Equil. Phase (°):</b>	-26	-30
<b>Shunt Imped. (MΩ/m):</b>	60-70	38-47
<b>Filling Time (μs):</b>	220	80
<b>No. Tanks:</b>	4	44
<b>Tank Diam.:</b>	94-88	26
<b>No. Drift Tubes:</b>	161	-
<b>Drift Tube Length (mm):</b>	49-373	-
<b>Drift Tube Diam. (mm):</b>	180-160	-
<b>Gap/Cell Length Ratio:</b>	0.21-0.41	-
<b>Iris Thickness:</b>	-	-
<b>Iris Spacing:</b>	-	-
<b>Aperture (mm):</b>	15-30	40
<b>No. Quads:</b>	134	104 doublets
<b>Gradient (T/m):</b>	77-5	20-30
<b>No. RF Power Units:</b>	4	44
<b>RF Power Input, Peak (MW):</b>	9.5	35
<b>Mean (MW):</b>	1.3	4.2 (9% beam df)

### Vacuum System

**Material of Vac. Chamber:** Copper and stainless steel  
**Aperture of Vac. Chamber:** -  
**Average Pressure**  $3 \times 10^{-8}$  torr  
**Pumps (No., Type, Speed):** 10 Ion pumps at 2400l/s and 133 Ion pumps at 600l/s

### Published Articles Describing Machine

See proceedings of recent accelerator conferences and LAMPF Users Handbook.

### ACCELERATOR PERFORMANCE

	Goal	Maximum Achieved
<b>Energy (GeV):</b>	0.8	0.8
<b>Resolution <math>\Delta E/E</math> (%):</b>	0.5	0.2
<b>Repet. Rate (pulse/s):</b>	120	120
<b>Pulse Width at Peak E:</b>	1000 $\mu$ s	750 $\mu$ s
<b>Duty Factor, Macroscopic (%):</b>	12	9
<b>Internal Beam (part/pulse):</b>	$5 \times 10^{13}$	$3 \times 10^{13}$
<b>(part/s):</b>	$6 \times 10^{15}$	$4 \times 10^{15}$
<b>Emittance at Peak E:</b>	$3 \pi$ mm-mrad (Emittance = Area $\times \beta\gamma$ at 90% current)	
<b>Other Data:</b>	-	

### SECONDARY BEAMS

Particle	Momentum Range	No. of Beams	Other Inform.
$\pi^{\pm}$	100-700 MeV/c	3	Up to $10^9 \pi^+/s$
$\pi^{\pm}$	125-400 MeV/c	1	For pion spectro.
$\mu^{\pm}$	0-250 MeV/c	1	$> 10^7 \mu^+/s$
$\pi^-$	150-200 MeV/c	1	For biomed. Appl.
p	1000-1500 MeV/c	2	Up to 50 nA
p	1000-1500 MeV/c	1	P1 $\div$ P4, P8 For high re. Spectro.
n	600-1500 MeV/c	1	-
$\nu_e$	20-50 MeV/c	1	-
p	1500 MeV/c	1	For pulsed neutron TOF experiments

### RESEARCH PROGRAMME

<b>Total Experimental Areas:</b>	4600 m <sup>2</sup>	<b>No. Ext. Targets:</b>	-
<b>No. Internal Targets:</b>	-		
<b>No. Separated Beams:</b>	-		
<b>No. Beams Served At Same Time:</b>	12		
<b>Total Power Used (Average) for Research:</b>	25 MW		
<b>No. User Groups:</b>	-		
<b>Total Research Staff:</b>	In house 25, outside 429		
<b>Ann. Research Budget:</b>	-		
<b>Annual Research Time:</b>	4000 h (1979)		

### Other Relevant Parameters or Notable Features

Simultaneous H<sup>+</sup> and H<sup>-</sup> beams are accelerated to full energy at same duty factor. Options on H<sup>-</sup> are reduced energy (to 400 MeV), polarized 10 nA or, unpolarized 5  $\mu$ A average current while H<sup>+</sup> beam is provided at 800 MeV, 600  $\mu$ A average current. Irradiation facilities in primary and secondary proton beam stops are provided for radiochemistry and isotope production.

### Recent Improvement or Modification to Machine

Increased average current and duty factor, variable energy H<sup>-</sup> and, polarized H<sup>-</sup>.

## EXTRACTION FROM THE CERN SPS

*Y. Baconnier, P. Faugeras, K.H. Kissler, B. de Raad, W. Scandale  
CERN, Geneva, Switzerland*

### 1. SUMMARY

The experimental programme requires three different modes of extraction from the SPS: fast extraction (burst duration from  $3\mu\text{s}$  to  $23\mu\text{s}$ ), slow resonant extraction (spill duration 0.5s to 2s) and fast resonant extraction (spill duration shorter than 3ms). All three modes have been successfully tested and brought into operation. Fast extraction of the full beam is 100% efficient. By fast beam shaving, fraction as low as 1% of the circulating beam can be extracted in a fairly stable way. Third-integer extraction is used to produce slow spills of 700 ms or more. The efficiency of resonant extraction is currently some 97%. The spill duty factor at present amounts to about 40%. Fast resonant spills of less than 2 ms were achieved with both integer and half-integer extraction. The different modes of extraction are consecutively performed during each accelerator cycle. At present, a 1s third-integer spill at 200GeV/c is followed by a fast shaving extraction at 210GeV/c and by fast or fast resonant extraction of the remaining protons at 400GeV/c.

### 2. EXTRACTION CHANNEL

The beam is extracted in the horizontal plane. The layout of the extraction channel is shown in Fig. 1 together with the mechanical aperture in the extraction region and beam envelopes for third-integer extraction.

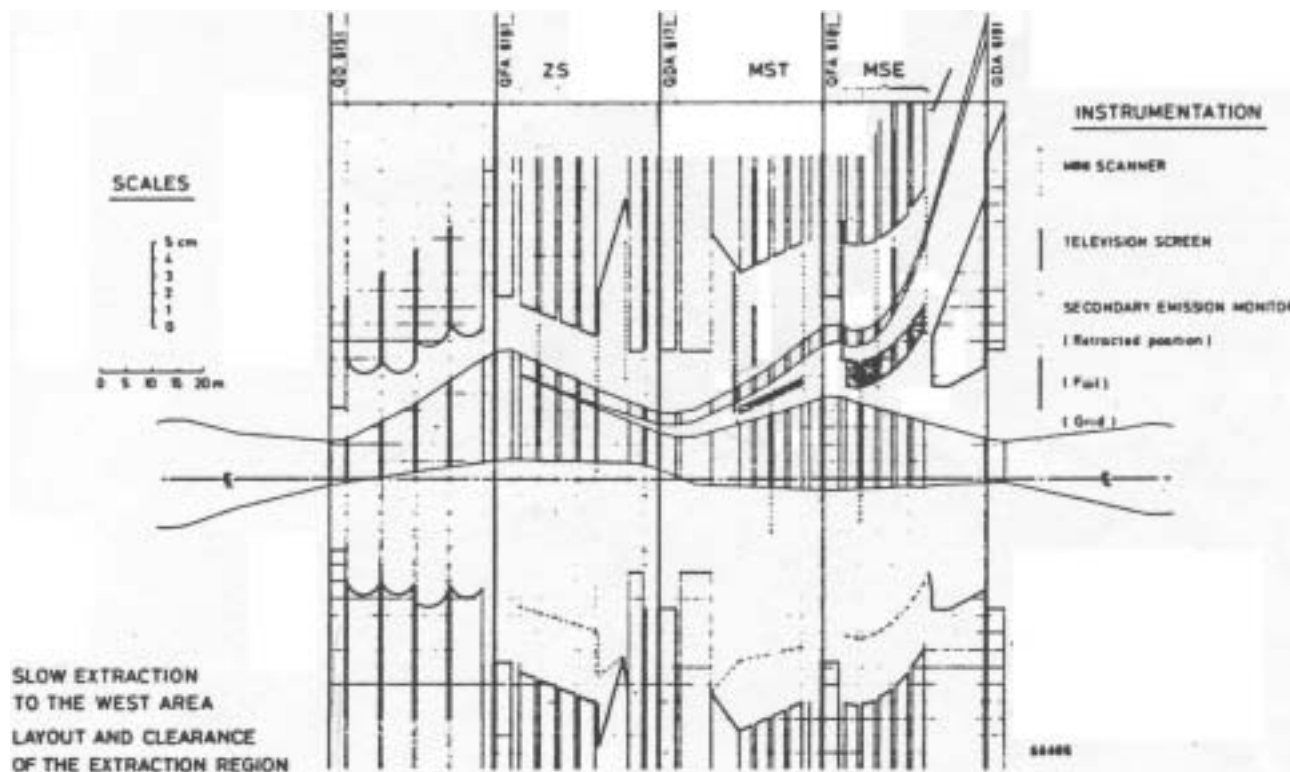


Fig.1 Layout of the SPS extraction channel

The first deflecting device of the extraction channel, the electrostatic septum ZS, is followed by two septum magnets MST and MSE consisting of several units each which bend the extracted protons away from the machine. The beam splitting plane of the electrostatic septum consists of a row of vertical tungsten wires with a diameter of 0.12 mm, spaced at 1.5 mm intervals. The wires are at ground potential. Parallel to the plane of wires an oxidized aluminium cathode can be remotely adjusted in a range from about 0 to 40mm. In general it is set to 20mm with a cathode potential at  $-200\text{kV}$ . The wires of the septum anode are spring loaded in such a way that broken wires are automatically retracted from the machine aperture. The electrostatic septum consists of 4 separate units, 3m long each. These units are aligned on a common support which can be remotely adjusted. In addition, individual remote adjustment of each of the 4 wire planes permits to minimize the extraction losses.

During extraction the closed orbit position and direction at each septum of the extraction channel are accurately controlled by a set of 5 horizontal and 4 vertical dipoles.

As indicated in Fig.1 a number of beam monitors have been installed along the extraction channel which permit detailed studies of the extraction process. Particularly, miniscanners give precise measurements of parameters like jump size and divergence of the resonant proton beam at the electrostatic septum or beam separation at the copper septa. These scanners consist of thin metallic flags that can be moved in steps through the beam. The positive charge of the flag created by the traversing protons yields a measure of the proton flux at the scanner position. The range of the scan, step size and number of steps, as well as the timing of the acquisition can be varied by a computer program over a wide range.

A total of 14 ionization chambers installed at crucial positions in the extraction channel allow to analyse the losses at the septa and to optimise the adjustment.

### 3. FAST EXTRACTION

Once the extraction channel has been adjusted, fast extraction is obtained by a rapid deflection of the beam with a pair of fast kicker located one quarter betatron wavelength upstream of the electrostatic septum. Protons which are not sufficiently deflected to jump the septum start a coherent betatron oscillation which is cancelled by another pair of kickers about one wavelength downstream of the first pair. In order to cope with different tunes of the machine, a fifth kicker is used for an optimal compensation of the kick and is located in between the two pairs. All five kickers have rise and fall times of about 900ns. They can give up to three kicks per machine cycle, each independently adjustable in amplitude and duration. The maximum deflection at the ZS entrance is 24 mm at 400GeV/c.

Two modes of fast extraction are used in operation:

1. Fast extraction of the full beam, obtained with a kick duration of 23.2 $\mu$ s. the extraction efficiency is 100% when the rise of the kickers is correctly synchronized with the 2 $\mu$ s hole in the circulating beam which results from injection.
2. Fast extraction of part of the beam, which is obtained by reducing the kick duration. Usually the kick amplitude is reduced in addition so that only a fraction of the beam cross section jumps the electrostatic septum ("shaving"). In this way it is possible to extract very small percentage of the circulating beam. With a kick duration of about 5 $\mu$ s and with 60% of the nominal deflection, fractions as low as 1% have been extracted. The extracted intensity fluctuated in this case by about 40% from cycle to cycle as only the edge of the beam profile was shaved off. For 2.5% extracted, the fluctuation are reduced to about 10% of the extracted intensity. Fig. 2 which was obtained with a fast digitising technique shows the circulating beam and the shaving of a fraction of 3%.

Recently a "learning programme" has been implemented which averages over a few cycles the extracted intensity and the acts on the kicker settings in order to keep the extracted percentage constant.

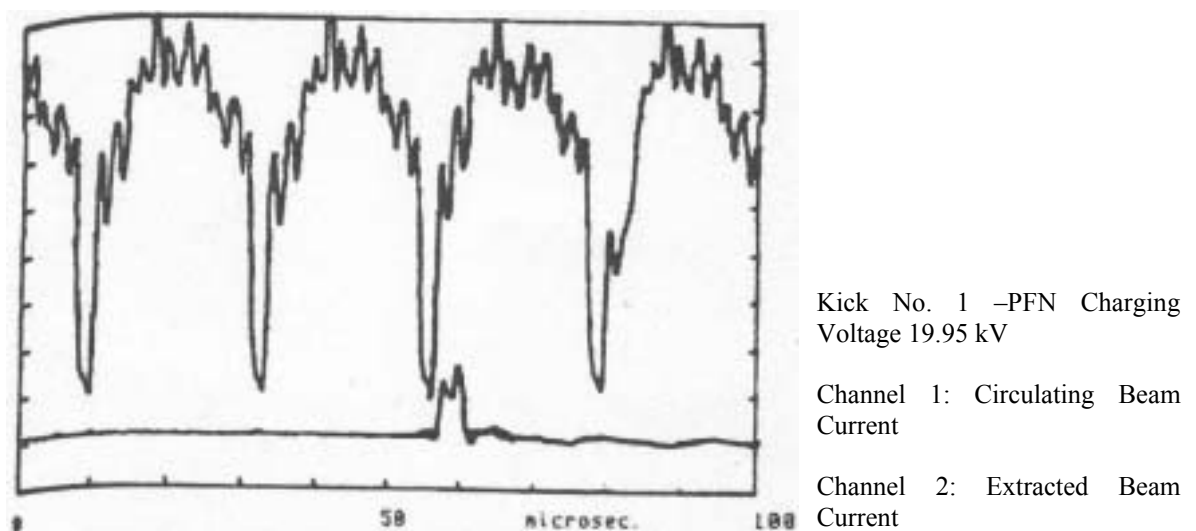


Fig. 2 Fast shaving extraction of 3% of the circulating beam

### 4. SLOW RESONANT EXTRACTION

Slow resonant extraction has been successfully tested at the following horizontal tunes: 27  $\frac{1}{3}$ , 27  $\frac{1}{2}$ , 27  $\frac{2}{3}$  and 28. these tests confirmed the prediction that integer and half-integer extraction are more sensitive to ripple on the various

magnet currents than third-integer extraction. Moreover, in the SPS  $\nu_H=27.4$  was found to be a better working point than  $\nu_H=27.6$ . (There is evidence for a 5<sup>th</sup> order structure resonance at  $\nu_H=27.6$  linked to the 6-fold symmetry of the accelerator). For these reasons slow resonant extraction is done at  $\nu_H=27 \frac{1}{3}$  in present operation and the results reported below refer to this resonance.

### Extraction procedure

The third-integer resonance at  $\nu_H=27 \frac{1}{3}$  is excited by 4 sextupoles, which are located in such a way that they create a field perturbation containing a strong 82<sup>nd</sup> harmonic with a suitable phase at the electrostatic septum. Protons are gradually brought into resonance by changing the current in the main machine quadrupoles to lower the radial tune.

Slow extraction is currently made on an intermediate 200GeV/c flat top, keeping the radio frequency (RF) on in order to allow for subsequent acceleration of the non extracted proton to top energy. To achieve a uniform spill a real time feedback system is used. The spill signal from a secondary emission monitor is compared with a reference signal. The difference between the two signals is amplified and acts on the radial position loop of the RF, changing the momentum and therefore the  $\nu$ -value of the beam.

### Extraction losses and efficiency

If the extraction channel is correctly adjusted, noticeable losses are only observed at the electrostatic septum. Figure 3 shows a typical density distribution at this septum (extracted protons are on the left of the wire plane indicated at position "0"). The density at the wires is some 12% per mm. This, together with an effective geometrical septum thickness of 0.2 to 0.25 mm (after careful adjustment of the 4 anodes) permits to deduce that present extraction losses are approximately 3%. No absolute measurement of the losses has been performed to date.

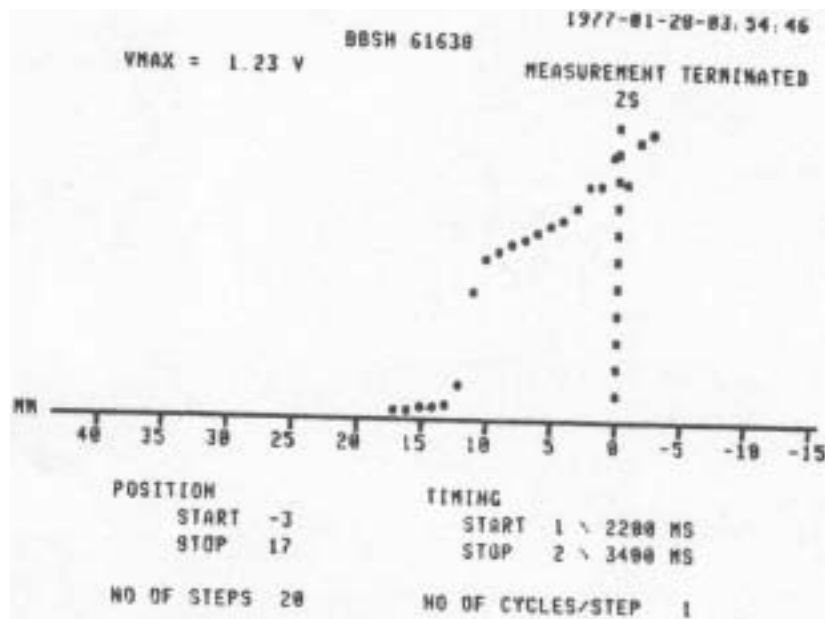


Fig. 3 Density distribution at the electrostatic septum ZS for slow resonant extraction.

### Spill duration, spill structure, beam survival

A typical spill is shown in Fig.4. Longer spills up to 2.7s duration have been achieved with a similar time structure. At present the duty factor for the slow spill is limited to about 40%. This limitation is mainly due to some residual magnet ripple, to an instability of the real time feedback system and to a high frequency time structure (frequencies greater than or equal to the SPS revolution frequency).

Whereas our initial effort was concentrated on the investigation of the different resonant extraction schemes and their relative merits, the main work is now directed towards an improvement of the spill duty factor.

It is typical for third-integer extraction that part of the protons survive the extraction process and emerge on the other side of the resonance. Beam survival of somewhat less than 10% is usually observed during operation with RF on (the surviving protons are subsequently fast or fast-resonant extracted during the same accelerator cycle).

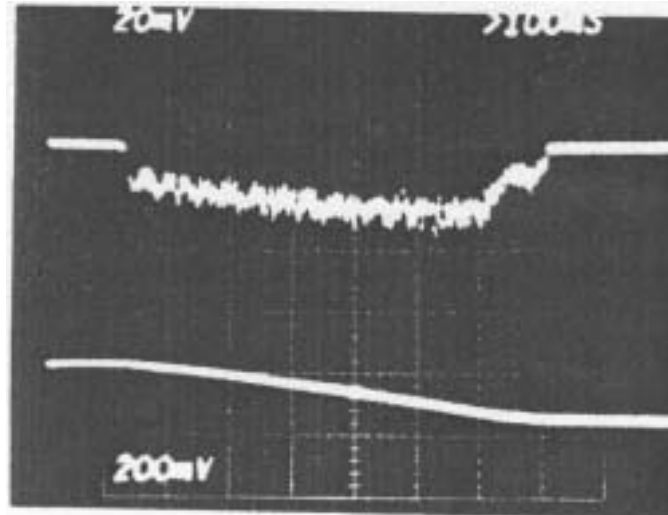


Fig. 4 Slow third-integer spill, controlled by a real time feedback system. Upper trace: Spill signal from a secondary emission monitor (100 ms/div). Lower trace: Integrated losses at ZS.

### Transverse beam properties

At 200 GeV/c the following emittances of the slow extracted beam are usually measured:  $\varepsilon_H \approx 0.15\pi$  mm mrad,  $\varepsilon_V \approx 0.15\pi$  mm mrad.

The horizontal emittance strongly depends on the RF voltage which is kept on during the flat top. At full voltage the emittance increases up to a factor of 10 compared to low RF voltage.

The extracted beam properties also strongly depend on the current in the Landau damping octupoles powered at higher intensities mainly to damp the head to tail instability in the SPS.

## 5. FAST RESONANT EXTRACTION

Fast spills of less than 2ms were successfully achieved with both integer and half-integer extraction. After excitation of suitable extraction lenses – one quadrupole and two sextupoles for integer extraction, one quadrupole and 4 octupoles for half-integer – the proton beam was rapidly brought into resonance by one half of the following methods:

For half-integer extraction the current in the machine quadrupoles was simply changed at the maximum possible rate and this resulted in the desired short spill.

For integer extraction two different ways were used to spill out the protons rapidly: The first method consists in displacing the beam in the extraction quadrupoles by switching the Rf off and changing the main magnet field. The resulting deflection in the extraction quadrupole strongly displaces the beam in the sextupoles which then yield the necessary  $\nu_H$ -shift. In the second method the required deflection at the position of the extraction quadrupole is made by a pulsed dipole field close to it. With this second method resonant spills as short as 700  $\mu$ s were obtained.

For a 2 ms integer spill the properties of the extracted beam are not noticeably different from those of a beam extracted within several 100 ms. For half-integer extraction the divergence at the electrostatic septum for a 2 ms spill is twice as large as for a long spill.

\* \* \*

## ACKNOWLEDGMENTS

Many people contributed to the construction of the SPS extraction system and to the successful running-in. The authors would like to thank them all. We particularly acknowledge the contributions of K. Bätzner, R. Bonvin, J. Bossler, G. Corazza, M. Cornacchia, R. Dubois, J. Dupin, R. Guinand, C. Harrison, H. Kuhn, V. Rödel and G. Schröder.

## INJECTION METHODS IN THE FERMILAB BOOSTER

*D.F. Cosgrove, C. Curtis, E. Gray, C. Hojvat, R.P. Johnson and C. Owen*  
*Fermi National Accelerator Laboratory\**  
*Batavia, Illinois 60510, USA*

### 1. SUMMARY

At present there are two working injection methods: single-turn using a ferrite kicker magnet and multiturn using a pulsed set of 4 dipoles in one straight section. The operating characteristics of these methods are described. The expected implementation of  $H^-$  injection will involve the incorporation of devices for all three methods in one 6-m long straight section. The  $H^-$  scheme is described and the expected operating characteristics compared to the present methods.

### 2. INTRODUCTION

A booster synchrotron, cycling at 15 Hz, receives 200-MeV beam from a proton linac and delivers 8-GeV beam to the main-ring synchrotron. There are certain limitations which restrict the performance of the booster. These include, among other things, the intensity, transverse emittance and momentum spread of the linac beam as well as the transverse and longitudinal acceptance of the booster. Residual radioactivity resulting from loss of injected beam also places a premium on efficiency of capture and transmission of the linac beam.

The original booster design<sup>1</sup> provided for multiturn injection, however, a single-turn kicker was added during construction. The design acceptances were  $90\pi$  mm-mrad,  $45\pi$  mm-mrad, and 3.0 eV-sec for horizontal, vertical and longitudinal acceptances respectively. These values are adequate to accept into horizontal phase space four turns of linac beam with transverse emittance in both planes of  $10\pi$  mm-mrad, and a momentum spread of  $\Delta P/P$  of  $\pm 0.9 \times 10^{-3}$ . A design linac<sup>1</sup> beam of 75 mA having these properties would then give in excess of  $5 \times 10^{13}$  protons per main ring pulse, the design goal, for 13 booster batches. These properties for the linac beam were in practice achieved for 90% of the beam<sup>2</sup>. On the other hand, the booster has achieved its design values for only the longitudinal acceptance, which necks down to this value at approximately 3 msec into the acceleration cycle. The operational acceptances are  $\sim 25\pi$  and  $16\pi$  mm-mrad<sup>3,4,5</sup> in the horizontal and vertical planes respectively. The vertical emittance is limited by the extraction septum.

Three methods of injection are discussed in this paper. Single-turn and multiple-turn injection have been used.  $H^-$  injection with stripping is in the planning stage.

### 3. MULTITURN INJECTION

After the early stage of booster operation with single-turn injection, multiturn operation was the rule<sup>2</sup>. Figure 1 shows the parallel displacement of the equilibrium orbit over to the wire septum of an electrostatic inflector by four orbit-bump dipole magnets. A pulsed septum magnet bends the incoming beam  $8.3^\circ$  before the final bend of  $0.7^\circ$  by the electrostatic inflector. The bump-magnet field was designed to decay at a rate of approximately one-half beam width per turn in order to stack beam in horizontal phase space. The original plane employed half-integral tune at injection. A more usual tune value in use is about 6.62.

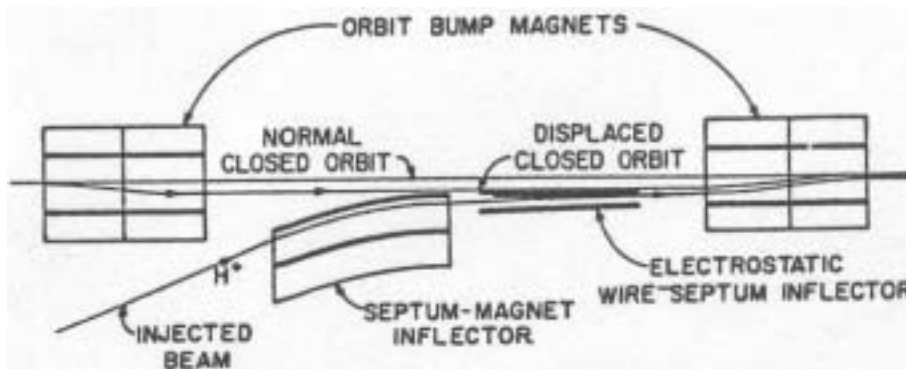


Fig. 1. Multiturn Injection System

The small radial acceptance has made capture of beam for more than three turns very efficient. Some beam intensities achieved from the booster transmission are shown in Table I. Maximum main-ring beam does not always correspond to

maximum booster beam. Much accelerator operation has used two-turn method, the beam is susceptible to loss vertically through coupling of the large radial amplitudes with vertical motion.

Table I  
Operational Intensity Records

<i>Injection Method</i>	<i>No. of Turns</i>	<i>Linac Current (mA)</i>	<i>Booster/Linac Efficiency (%)</i>	<i>Max. Booster Intensity (<math>10^{12}</math>)</i>	<i>Date</i>	<i>Max. main Ring Intensity (<math>10^{13}</math>) 13 Booster Batches</i>	<i>Date</i>
Orbit Bump	4	85	29	1.71	6-10-75	1.75	6-10-75
	3	115	36	2.12	12-8-75	1.73	12-8-75
	2	150	37	1.93	1-20-76	2.02	1-20-76
Single-Turn Kicker	1	265*	50	2.33	12-11-76	2.48	1-20-76
H <sup>-</sup> Stripping	≥20	30	-	-	-	-	-

\* maximum current is 300 mA for 4 μsec pulse.

#### 4. SINGLE-TURN INJECTION

The same electrostatic inflector and septum magnet in Fig. 1 are used for single-turn injection and, in principle, no orbit-bump magnets are required. The incoming beam upon entering the booster is parallel to the closed orbit and displaced outward from it. Approximately one-quarter betatron wavelength downstream, in the next long straight section, a ferrite kicker removes the crossing angle at the central orbit. In practice, for much of the single-turn operation, a bump was placed in the closed orbit in the region of injection by four dc trim dipoles. This bump permitted careful alignment of the injection orbit and displacement of the orbit toward the inflector from which it returned to its normal position during acceleration. More recently the pulsed orbit-bump magnets are used to provide part of this orbit displacement so that the bump is more localized and the orbit moves faster back to its normal position.

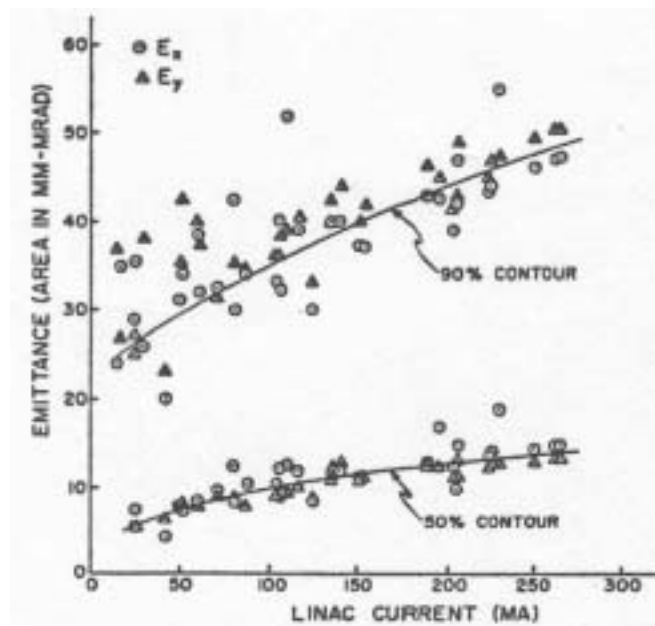


Fig. 2. Linac emittance as a function of current for a variety of operating conditions.

Because of the greater booster transmission efficiency for single-turn over multiturn injection, a serious study of single-turn injection for higher linac beam current began in January 1976. It was possible at the time to operate at currents to 160 mA for short beam pulses. Momentum slewing because of insufficient rf power in the linac was compensated by the debuncher, which also reduced the increased momentum spread resulting from space charge. This immediately gave beam from the booster (and main ring) in excess of 80% of the intensity obtained by multiturn injection. In the months that followed, operation alternated between single-turn and two-turn injection while modifications to the column of the Cockcroft-Walton accelerator were in progress to increase further the linac beam current. Use of single-turn injection exclusively since last fall has given record 8-GeV and 400-GeV intensities (See Table I) of  $2.3 \times 10^{12}$  protons per booster cycle and  $2.5 \times 10^{13}$  protons per main-ring cycle.

Measured linac emittance typically has increased with increasing beam current but slowly enough that the brightness increases. This behaviour favors high-current single-turn injection. Linac currents up to 300 mA in a pulse length of 4  $\mu$ sec have been achieved. See Fig. 2 for an accumulation of operating emittance values over a period of time for three variations of the accelerating column.

Figure 3 shows an accumulated record of operating booster transmission as a function of beam current for single-turn injection. Note the linear upper boundary of the booster transmission.

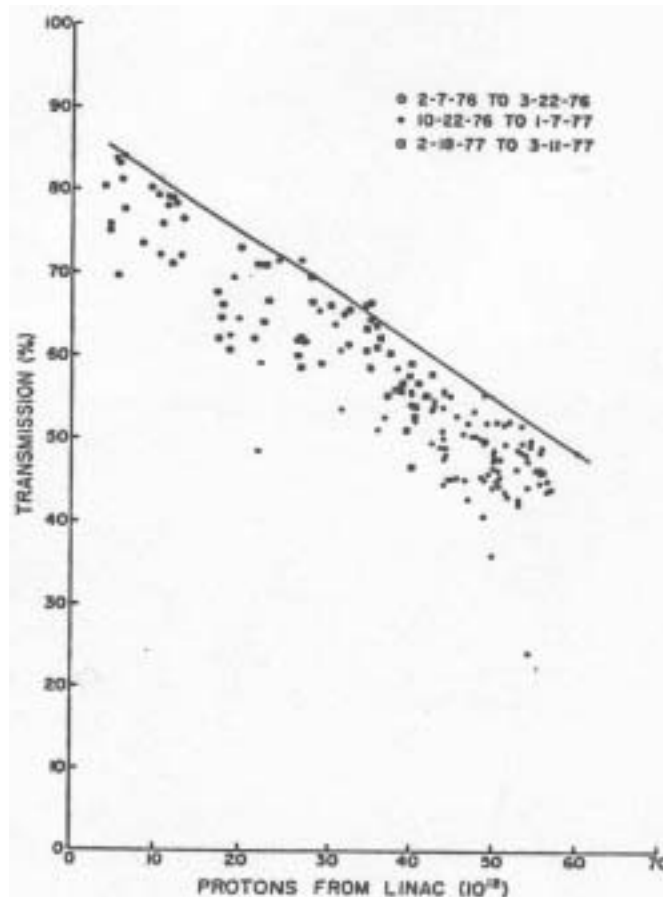


Fig. 3. Booster efficiency measured as the ratio of 8-GeV beam to 200-MeV beam out of the linac for single-turn injection. The solid curve represents the approximate maximum transmission attainable.

### 5. H<sup>-</sup> INJECTION

Increase in phase-space density by stripping the two electrons from H<sup>-</sup> beam injected for many turns on the same orbit, long suggested, has been demonstrated nicely at Argonne<sup>6,7</sup>. The injection process as envisioned at Fermilab is shown in Fig. 4. The same long straight section will be used for either H<sup>+</sup> or H<sup>-</sup> injection by using some of the same magnets in both cases. A third pair of orbit-bump magnets will change places with the electrostatic deflectors for H<sup>-</sup> injection as shown. The orbit is held fixed during injection and is returned to its normal position during the first few turns after injection. An example of the numbers involved to reach the design goal,  $5 \times 10^{13}$  protons per cycle out of the main ring, is as follows. If we assume 80% transmission of the main ring, 50% transmission of the booster and 90% stripping efficiency, a linac beam of 30 mA will require about 21 turns or a linac pulse length of about 58  $\mu$ sec. For this stripping efficiency, a foil of the Argonne variety (mostly carbon) has a thickness of about 300  $\mu$ gm/cm<sup>2</sup>. It will produce a trivial energy loss of 1 keV/turn and produce an rms scattering angle of less than  $\frac{1}{2}$  mrad for those protons longest on the foil. If we assume a linac emittance of  $10\pi$  mm-mrad, the growth in emittance for a matched beam due only to multiple scattering is approximately 6% and 22% in the horizontal and vertical planes respectively<sup>8</sup>.

A few foils prepared at Argonne have been tested in the 200-MeV circulating beam of the booster<sup>9</sup>. The thinner foils tend to confirm the lifetime of  $\sim 10^{18}$  protons achieved at Argonne. A multiple-foil holder and changer is required.

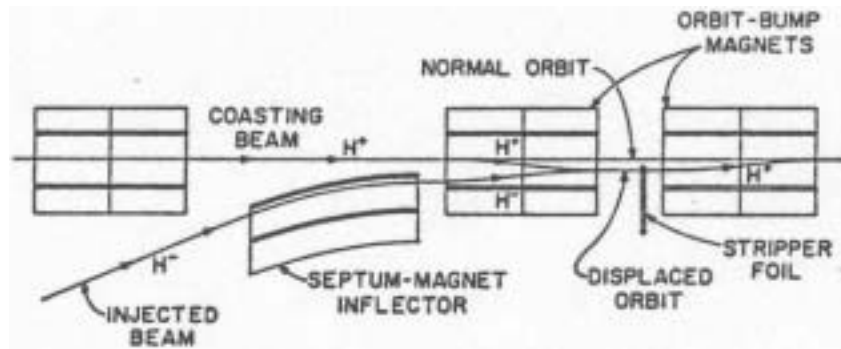


Fig. 4.  $H^-$  injection system

## 6. COMPARISON AND CONCLUSIONS

Single-turn injection proves a practical competitive scheme for sufficiently high linac-beam intensity. It has yield ~25% more beam intensity at 400 GeV than the multturn injection. In addition, the efficiency of single-turn injection is much higher and leads to less residual radioactivity. Linac beam currents greater than 250 mA have rarely been used because of little gain in booster intensity at these levels but more importantly because of increased booster beam size which the main ring cannot accept. These facts as well as the linear fall off of booster transmission with increasing current and other data suggest space charge limited performance within the available booster acceptance. A recent experiment which detailed the beam loss over a large time interval during the acceleration cycle, for which the maximum energy was 4 GeV, also points toward this conclusion.

In view of the possible approach to the space-charge limit from incoherent tune shift, it is difficult to predict great improvement in performance with  $H^-$  injection, without further improvement in the booster's transverse acceptance. The smaller momentum spread and emittance in the injected  $H^-$  beam, however, should prove some advantage.

\* \* \*

## ACKNOWLEDGMENTS

The authors wish to recognize the assistance of Mr. J. Lackey and Mr. K. Meisner in the injection studies, dr. L. Teng in design studies of  $H^-$  beam transport and Mr. M. Joy in stripping technique studies and foil testing. They recognize also the great role played by the accelerator division who have contributed to continuing improvements in the booster and to increase of the linac beam intensity.

## REFERENCES

1. National Accelerator Design Report, Universities research Association, Batavia, Ill (1968)
2. C.D. Curtis and C.W. Owen, "Operation of the Fermilab 200-MeV Proton Linac", Proc. of the Fourth All-Union National Conf. on Particle Accelerators, Vol.1, P.136, Moscow, U.S.S.R. (1974)
3. Paul J. Reardon, "Status of the Fermilab 400-GeV Accelerator", Proc. of the Fourth All-Union National Conf. on Particle Accelerators Vol.1, p25, Moscow, U.S.S.R. (1974)
4. E.R. Gray et. al., "Transverse Beam Motion in the Fermilab Booster Accelerator", IEEE Trans. Nuclear Sci. NS-22 1900 (1975)
5. E.R. Gray et. al., "Longitudinal Beam Motion in the Fermilab Booster Accelerator", IEEE Trans. Nuclear Sci. NS-22 1897 (1975)
6. J.D. Simpson, "Operating Results from the ANL Booster", IEEE Trans. Nuclear Sci. NS-20 198 (1973)
7. Charles Potts, "Negative Hydrogen-Ion Injection into the ZGS", proceedings of his conference.
8. C. Schmidt and C. Curtis, "Negative Hydrogen-Ion Program at Fermilab", Proc. of the 1976 Proton Linear Accelerator Conf., Chalk River, Ontario, p.402
9. Marshall Joy, "Charge Changing Methods for  $H^-$  Injection into the Booster Synchrotron", fermilab internal report TM-699 (1976).

\* Operated by Universities Research Association Inc. under contract with the Energy Research and Development Administration.

## ELEMENTARY DESIGN AND SCALING CONSIDERATIONS OF STORAGE RING COLLIDERS

Alexander W. Chao

SSC Central Design Group, Berkeley, California 94720

### ABSTRACT

This article is a compilation of some considerations encountered in the design of storage ring colliders. It consists of two chapters. The first chapter describes an approach to the collider design from a particular point of view at an elementary level. The second chapter discusses a few semi-empirical scaling properties in the collider parameters.

### 1. ELEMENTARY DESIGN CONSIDERATIONS

In this chapter, the design of a storage ring collider is described from a particular point of view. We begin with the luminosity requirement on the collider and proceed to describe the various design features needed to provide the luminosity. Design features chosen to be discussed follow from the viewpoint chosen. No attempt has been made to cover all important features in a collider design. For illustration, a numerical example is carried along with the discussion. To avoid possible confusion the general equations are arranged in a numerical sequence: Parameters used in the numerical example are arranged in an alphabetical sequence.

#### 1.1 Luminosity

The end product of a storage ring collider can be summarized by three parameters: the type of particles, the particle energy  $E$  and the luminosity  $L$ . The type of particles is most likely electron or proton. In the following discussions, we assume that the particle type and particle energy are given and begin by a discussion on luminosity. Consider a certain type of high energy physics events of interest with cross-section  $\Sigma$ . The counting rate  $R$  of these events in a collider is proportional to  $\Sigma$ . The proportionality constant is called the luminosity, i.e.

$$R = L\Sigma \quad (1)$$

Consider two bunches with  $N$  particles each colliding head-on. Let the beams have a uniform transverse distribution with area  $A$ , as shown in Fig. 1. Let  $f$  be the frequency for collisions occurring at the collision point under consideration. Luminosity is given by

$$L = \frac{Nf^2}{A} \quad (2)$$

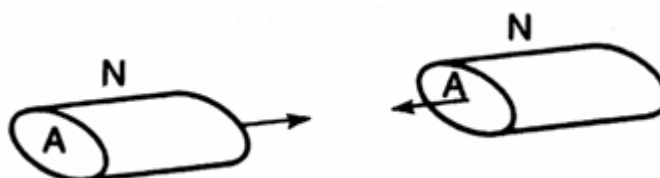


Figure 1. Two colliding bunches.

The collision frequency is related to the revolution frequency  $f_{rev}$  by:

$$f = f_{rev}B \quad (3)$$

where  $B$  is the number of bunches in each beam. In case the two beams have a round gaussian distribution in the transverse dimensions with rms size  $\sigma$ , the effective beam area is<sup>[1]</sup>

$$A = 4\pi\sigma^2 \quad (4)$$

It is sometimes convenient to remove the factor  $N^2$  from the luminosity expression (2). The remaining quantity is called the specific luminosity. It depends only on the overlapping geometry of the two transverse distributions and is independent of beam intensities, type of events, particles type and beam energy.

As a numerical example, consider an event type with  $\Sigma=1$  picobarn= $10^{-36}$   $cm^2$ . Suppose a counting rate of  $R=1/\text{day}$  is required on this particular event type, the needed luminosity is

$$L = \frac{R}{\Sigma} = 10^{31} \text{ cm}^{-2} \text{ s}^{-1} \quad (a)$$

To achieve this luminosity, a possible set of parameters is

$$\begin{aligned} N &= 10^{11} \\ f_{rev} &= 10^5 \text{ s}^{-1} \end{aligned} \quad (b)$$

$$A = 0.01 \text{mm}^2$$

$$B = 1$$

The probability that a particle actually collides with a particle in the on-coming beam is  $P=N\Sigma_{\text{tot}}/A$ , where  $\Sigma_{\text{tot}}$  is the total cross-section of collision. Assuming  $\Sigma_{\text{tot}}=100 \text{mb}=10^{-25} \text{cm}^2$ , the probability of collision is found to be  $10^{-10}$  per crossing. The lifetime of the beam due to actual collisions is thus  $10^{10}$  crossings, which corresponds to  $10^5$  sec, or about 1 day, since we assumed a revolution period of  $10^{-5}$  sec.

### 1.2 Beam-Beam Effects

We found that the probability of actual collision is extremely small per crossing, meaning the bunch is basically transparent as far as particle crossing is concerned. However, particle motion across the collision points is by no means unperturbed. The perturbation comes from the elastic scattering by the collective Coulomb field associated with the on-coming bunch. This perturbation is referred to as the beam-beam interaction.<sup>[2]</sup>

The beam-beam interaction constitutes one of the main limiting effects on the luminosity. To achieve a high luminosity, one needs a high beam intensity and a small beam area. These requirements must be made so that the beam-beam effect is not made intolerably strong.

First let the transverse beam distribution be a uniform disc with radius  $a$ . Consider a test particle in beam 1 that passes through beam 2 with a transverse displacement  $x$  from center, as shown in Fig. 2. In the ultra-relativist limit, the electric field seen by the test particle points in the radial direction perpendicular to its direction of motion. Applying the Gauss law yields

$$\varepsilon_r = \begin{cases} \frac{2Ne}{l} \cdot \frac{x}{a^2} & \text{if } |x| < a \text{ uniform disc} \\ \frac{2Ne}{l} \cdot \frac{a}{x} & \text{if } |x| > a \end{cases} \quad (5)$$

where  $l$  is the length of the beam bunch

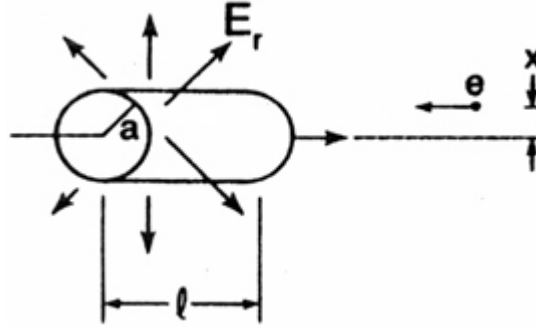


Figure 2. the beam-beam encounter seen by a test charge

In addition to the electric field, there is a magnetic field  $B_0$  of the same strength (in cgs units) as the electric field. The Lorentz forces due to the electric and the magnetic fields add to give a force twice that due to the electric field alone. Continuing our numerical example with  $N=10^{11}$  and  $A=\pi a^2=0.01 \text{mm}^2$  and take  $l=10 \text{cm}$ , the electric field is found to be  $50 \text{MV/m}$  and the magnetic field is  $1.5 \text{kG}$  evaluated at the edge of the beam,  $x=a$ , where the fields are maximum.

In case of a round gaussian distribution, the electric field is

$$\varepsilon_r = \frac{2Ne}{l} \left( \frac{1 - e^{-\frac{x^2}{2\sigma^2}}}{x} \right) \text{ round gaussian} \quad (6)$$

The beam-beam interaction imposes limitation on luminosity not because it is extraordinarily strong but because it is extraordinarily nonlinear. The linear part of the force acts like a quadrupole magnet, whose effect can be compensated by adjusting the strengths and arrangements of the neighboring quadrupoles. In particular, for the case of gaussian distribution, the linear force gives rise to a beam-beam tune shift given by<sup>[2]</sup>

$$\xi = \frac{Nr_0\beta^*}{4\pi\sigma^2\gamma} \quad (7)$$

where  $\beta^*$  is the  $\beta$ -function at the interaction point,  $\gamma$  is the relativistic factor,  $r_0$  is the classical radius of the particle type under consideration. Unlike the linear part, the nonlinear part of the beam-beam force is not so easy to deal with. Fig.3 shows the beam-beam force as a function of  $x$  for gaussian and uniform disc beams. The nonlinearity starts around  $x>\sigma$  for the gaussian case. For the uniform disc case, the force inside the beam distribution is strictly linear. No particle feels

the nonlinearity since the nonlinear region is not populated. If beams can be prepared with strictly uniform disc distribution at the collision points, it follows that it will be no beam-beam problem. However, there are two potential obstacles to this idea that we will only mention here. One is obviously the practical difficulty to provide a uniform disc beam. The other is that there is another type of beam-beam interaction – the type that involves coherent motion of the bunches – that perturbs beam motion; uniform disc beams are not exempted from the coherent beam-beam effects.

To compare the nonlinearity of the beam-beam force with that of a multipole magnet field error, note that the beam-beam force deviates from linearity at a transverse distance of the order of the beam size at the interaction point (of the order of 0.1 mm) while a magnet field nonlinearity has the characteristic distance of the magnetic coil or gap size (of the order of centimetres).

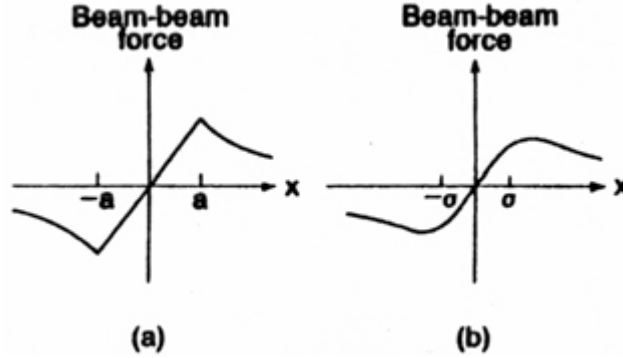


Figure 3. Beam-beam force as a function of the transverse displacement of the test particle for (a) a uniform disc beam and (b) a round gaussian beam

It turns out that the strength of the beam-beam non linearity is specified by the same quantity that specifies the linear part of the beam-beam force, namely the beam-beam tune shift  $\xi$ . To control the beam-beam nonlinear effects, it is therefore necessary to limit  $\xi$ . One of the fundamental constants in the design of a storage ring collider is in fact the maximum  $\xi$  that allows stable motion of particles in the presence of the nonlinear beam-beam perturbation. For the purpose of our discussions, we assume without elaboration that the beam-beam limit is reached at

$$\xi_{limit} = \begin{cases} 0.005 & \text{for protons} \\ 0.05 & \text{for electrons} \end{cases} \quad (8)$$

By comparing the expressions (2) and (7), the condition imposed by the beam-beam limit puts a limit on gaining luminosity by increasing N and decreasing A. However, there is still the factor  $\beta^*$  in expression (7) free to be used for optimisation.

To proceed, we need to consider the condition imposed by the beam emittance. For a round beam, the emittance is given by

$$\varepsilon = \frac{\sigma^2}{\beta^*} \quad (9)$$

For protons,  $\varepsilon$  is inversely proportional to  $\gamma$  due to the adiabatic damping. For electrons,  $\varepsilon$  is proportional to  $\gamma^2$  due to quantum emission effects<sup>[1]</sup>. For a given beam energy, we assume for now that the beam emittance is given. The luminosity and the beam-beam tune shift are then rewritten as

$$\begin{cases} L = \frac{N^2 f}{4\pi\varepsilon\beta^*} \\ \varepsilon = \frac{Nr_0}{4\pi\varepsilon\gamma} \end{cases} \quad (10)$$

The only free variable that appears in  $\xi$  is the number of particles per bunch N. take a proton storage ring for example, we may have a normalized emittance  $\varepsilon\gamma=2\times 10^{-6}$  m-rad, the beam-beam limit is reached at  $N=10^{11}$ , i.e.

$$\xi = 0.005 \quad (c)$$

With N given, luminosity can still be improved by increasing the number of bunches per beam B and by decreasing  $\beta^*$ . A small  $\beta^*$  decreasing is beneficial because (a) it makes the beam area A small which in turn makes higher luminosity and (b) it makes particle motion less sensitive to the nonlinear beam-beam perturbation. In the following, we will set  $B=1$  and concentrate on the choice of  $\beta^*$ .

### 1.3 Low- $\beta^*$ Insertion

We have assumed in our numerical example a revolution frequency of  $f_{\text{rev}}=10^5 \text{ sec}^{-1}$ . This means the storage ring has a circumference of 3 km or the ring radius is about 500 m. For a superconducting proton storage ring, this means a beam energy of 500 GeV using a scaling property to be discussed in the next chapter, i.e.

$$\begin{cases} R = 500m \\ E = 500GeV \end{cases} \quad (d)$$

The value of  $\gamma$  is therefore about 500 and beam emittance is

$$\varepsilon = \frac{2 \times 10^{-6} m - rad}{500} = 4 \times 10^{-9} m - rad \quad (e)$$

Substituting in Eq. (10), we find that the design goal of  $L=10^{31} \text{ cm}^{-2}\text{sec}^{-1}$  can be reached if

$$\beta^* = 0.2m \quad (f)$$

This value of  $\beta$ -function at the interaction point is to be compared with the average  $\beta$ -function in the storage ring. For a storage ring with 500 m radius, as will be explained in the next chapter, the average  $\beta$ -function is approximately given by

$$\langle \beta \rangle = 22m \quad (g)$$

We thus conclude that there needs to be a special lattice insertion consisting of a sequence of quadrupole magnets to focus the  $\beta$ -function from an average value of 22 m down to 0.2 m at the interaction point. This special insertion – the low- $\beta^*$  insertion – is an important invention that has strongly enhanced the luminosity of storage ring colliders.<sup>[3,4]</sup> The price to pay is that it also makes the optics of the storage ring quite strained, as will be discussed next.

#### 1.4 Optical Aberrations Due To Small $\beta^*$

There are several limitations in reducing  $\beta^*$  indefinitely in order to gain luminosity. Practical limitation on the strength of the low- $\beta^*$  insertion quadrupole magnets is one example. Another limitation is that  $\beta^*$  should not be smaller than a length of the order of the bunch length.<sup>[5,6]</sup> These limitations, however, will not be discussed below. Instead, we discuss a third limitation, i.e. the aberration of the storage ring optics caused by the low- $\beta^*$  insertions.

At the start, a storage ring is composed of bending magnets and quadrupole magnets – bending magnets to guide the trajectory of particles and quadrupoles to provide the focusing. The  $\beta$ -function around the storage ring is sketched in Fig. 4. The insertion has produced a small  $\beta^*$  at the interaction point, but it also produces a large  $\beta$ -function, which we assume to be  $\beta=500$  m, at the insertion quadrupole magnets.

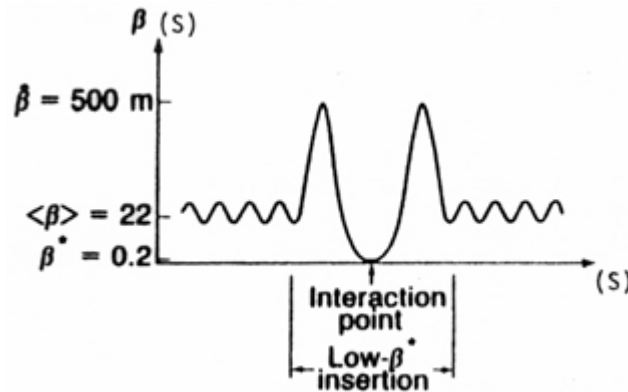


Figure 4. Sketch of the  $\beta$ -function in a storage ring collider.

If the particles in the beam do not have any energy spread, a storage ring consisting of only bending and quadrupole magnets will satisfactorily produce the behaviour shown in Fig. 4 and there will be no optical restriction on indefinitely reducing  $\beta^*$ . The motion of particles may be wild going through the variation of  $\beta$ -function but the motion is linear and is perfectly stable.

The difficulty arises when the beam has a finite energy spread. The low  $\beta^*$ , and thus the large  $\beta$  at the strong insertion quadrupoles, has associated with it a strong chromatic optical aberration. To see that, consider the effect of a quadrupole magnet on the motion of an off-momentum particle with energy error  $\delta=\Delta E/E$ . the kick angle is given by

$$\Delta x' = kx = \frac{k_0 x}{1 + \delta} = k_0 x (1 - \delta + \delta^2 - \dots) \quad (11)$$

where  $k_0$  is the quadrupole gradient seen by an on-momentum particle. The factor  $1/(1+\delta)$  represent the rigidity in the kick to the off-momentum particle under consideration. This rigidity factor is expanded in Eq. (11) into a power series to show its nonlinear behaviour in  $\delta$ . It is very nonlinear even if it may not look so.

One consequence of Eq. (11) is that the betatron tunes for an off-momentum particle will be different from the on-momentum values. In particular, one can define a quantity called chromaticity  $\nu'$  to be the linear variation of tune with  $\delta$ , i.e.

$$\nu = \nu_0 + \nu' \delta + \dots \quad (12)$$

In a storage ring with only bending and quadrupoles magnets,  $\nu'$  tends to be negative because the focussing effect provided by the quadrupoles is weaker for a higher energy particle. There are of course two chromaticities, one for the horizontal tune and one for the vertical tune.

It is mathematically possible to design a storage ring with only bending and quadrupole magnets and achieve  $\nu'=0$ . These designs however tend to give unacceptably strong nonlinearities in higher orders in  $\delta$ . So far no such design has yet been regarded as practical.

Take now an electron storage ring collider for example. As we will discuss in the next chapter, the rms beam energy spread almost always is of the order of  $\sigma_\delta=10^{-3}$ . Furthermore, in electron storage rings, the momentum aperture needed is of the order of  $10\sigma_\delta$  for the purpose of maintaining a good quantum lifetime<sup>[1]</sup>, leading to a needed total energy span of about  $\pm 1\%$ .

The finite energy spread, together with a finite chromaticity, gives a finite spread in the tunes. Since the tune spread in a storage ring is limited to avoid resonances, we need to impose the condition

$$|\nu' \delta| \leq 0.03 \quad (13)$$

the absolute value of the chromaticities must not exceed a value of the order of 3 or so.

There is another restriction on the chromaticity due to the head-tail instability effect<sup>[7,8]</sup>, which we will not elaborate on. To avoid the head-tail instability of beam motion, it is necessary to have a positive chromaticity, in conflict to the natural tendency. The range of acceptable chromaticity is thus approximately  $0 < \nu' \leq 3$ .

A low- $\beta^*$  insertion contributes to the chromaticity a term approximately given by

$$\nu' = \frac{1}{2\pi} \sqrt{\frac{\beta}{\beta^*}} \text{ per insertion.} \quad (14)$$

The smaller we make  $\beta^*$ , the higher  $\beta$  becomes, and the larger the chromaticity contribution from each insertion. In our numerical example, there is a chromaticity contribution of about  $-10$  from each insertion, which is large and negative.

In a storage ring consisting of only bending and quadrupole magnets, therefore, the on-momentum particles enjoy a purely linear motion and no instability limit but the motion of an off-momentum particle will most likely be unstable because of unfortunate tunes. Fig. 5(a) shows schematically the stable region in an aperture diagram.

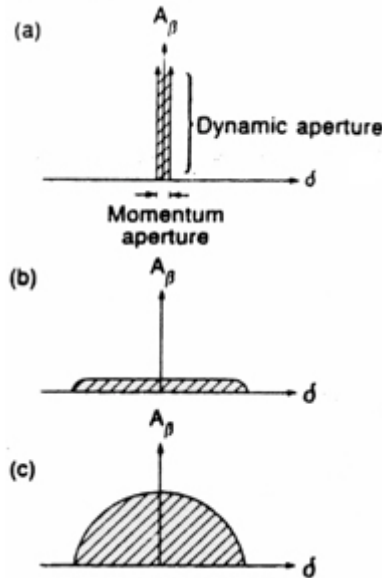


Fig. 5 Aperture diagram for a storage ring that consists of (a) dipole and quadrupole magnets only, (b) dipole, quadrupole and sextupole magnets, and (c) same as (b) but with special sextupole arrangements.  $A_\beta$  is the betatron amplitude,  $\delta$  is the relative energy error. Shaded regions indicate region of suitable motion.

In the aperture diagram, the maximum stable betatron amplitude is called the dynamic aperture. The maximum stable energy width is called the momentum aperture. Fig. 5(a) shows an infinite dynamic aperture and a very small momentum aperture in the case when the ring consists of only bending and quadrupole magnets. The momentum aperture is too small to be accepted.

### 1.5 Sextupoles

The question is then how to control the chromaticities. The answer is to install sextupole magnets in the storage ring. Sextupoles have the property that they act like quadrupoles when the center of the beam passes through them off-centered horizontally. We recall that a particle with  $\delta \neq 0$  has its closed orbit displaced horizontally by an amount  $\eta\delta$ , where  $\eta$  is the horizontal dispersion function. The kick given by a sextupole is therefore

$$\Delta x' = S(x + \eta\delta)^2 = Sx^2 + 2S\eta x\delta + S\eta^2\delta^2 \quad (15)$$

There are three terms in Eq. (15): one good, one bad and one irrelevant. The good term is the middle one which is linear in  $x$ , providing a quadrupole type of action and contributing an additional term to the chromaticity. If the sextupole polarities are such that its equivalent quadrupole field is defocusing for particles with  $\delta > 0$  and focussing for  $\delta < 0$ , it is possible to make the net chromaticity small and positive. The momentum aperture is thus be at least 2 sextupole families. The third term in Eq. (15) gives rise to a dispersion second order in  $\delta$ . We do not consider its effect here.

The bad term is the first term in Eq. (15). It produces a serious side effect due to its nonlinear nature in  $x$ . As a result, although we have compensated a large fraction of the chromatic aberrations, we have introduced new nonlinearities in the  $x$  variable, which substantially suppress the dynamic aperture. The situation is sketched in Fig. 5 (b). the achieved stable region is still not acceptable.

### 1.6 Sextupole Schemes

It is possible to improve the situation substantially by cleverly choosing the locations and strengths of the sextupoles. The idea is to make the sextupole nonlinearities cancel among themselves to a large extent. There are a few schemes to do that but we will describe one that is particularly simple, namely the achromat scheme.<sup>[9]</sup>

The spirit of the achromat scheme can perhaps be summarized by the simple principle of always forming pairs. In other words, if a sextupole is needed in the lattice, do not insert one sextupole; insert a pair instead. A properly arranged sextupole pair has much less nonlinear content than a single sextupole alone.

To make a sextupole pair, the two sextupoles of equal strength are spaced by a  $-1$  transformation in the betatron motion, as shown in Fig. 6. It is easy to show that if a particle enters the first sextupole with coordinate and slope of  $(x_0, x'_0)$ , the coordinate and slope of the particle as it exits the second sextupole is  $(-x_0, -x'_0)$ , independent of the existence of the sextupoles. The nonlinearities effects of the sextupoles thus cancel each other as far as the betatron motion (the bad term) is concerned. On the other hand, the focussing effect for off-momentum particles (the good term) can be arranged to be additive between the two sextupoles, yielding the needed chromaticity control.

Fig. 5(c) shows the aperture diagram when sextupoles are arranged to minimize their betatron nonlinear effects. The arrangement does not affect the momentum aperture much but increases the dynamic aperture substantially. Hopefully the operation region needed by the beam is inside the stable region finally achieved.

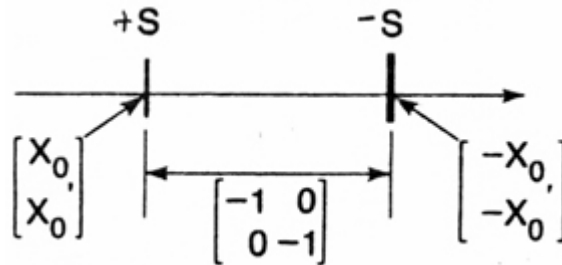


Figure 6. A sextupole pair used in the achromat scheme.

### 1.7 Recap

We started the discussion with the end product, in particular the luminosity, requirements. Particle dynamic was introduced by asking the question: what does a particle experience as it collides with the on-coming beam? The beam-beam interaction was then discussed. It was pointed out that the beam-beam interaction is a highly nonlinear effect. To limit its damage to the beam stability, a low- $\beta^*$  insertion is needed around each collision point. It was found that this low- $\beta^*$  insertions have severe side effects; they cause strong chromatic aberration which impose on the rest of the lattice design. To compensate for the chromatic aberrations, sextupoles are needed. The sextupoles in turn have their unfortunate side effects; to minimize those effects, it is necessary to arrange the sextupoles according to some clever scheme.

The design of a storage ring collider obviously does not stop here. The discussions offer only a possible elementary view, with its over-simplifications, of the design effort from a particular angle of single particle dynamics. To proceed further along this line, it is necessary to discuss another source of optical aberration, i.e. that from the magnet field errors. After that, there is the study of the effects due to the magnet alignment errors. Then there are issues such as how to make a closed orbit, dispersion function,  $\beta$ -function and linear coupling corrections. One shortcoming in discussing the design along this direction is that the important subject of collective effects is not discussed.

## 2. SOME SCALING PROPERTIES

### 2.1 Three Scaling Laws

In the previous chapter, we have carried along a numerical design example of a proton storage ring. We assumed it has a radius of  $R=500$  m. we mentioned in Eqs. (d) and (g) that for a storage ring of this size, the beam energy is going to be 500 GeV, average  $\beta$ -function is 22 m. We also mentioned that an electron storage ring collider will have an rms energy spread of  $\sigma_\delta=10^{-3}$ , regardless of its energy or size. These results are explained in this chapter by a few general scaling properties of storage ring collider parameters.

We first list three scaling laws together with the “experimental data” that confirm them. A few corollaries are derived from these laws. We then give the “mathematical proofs” of these laws. No attempt to be rigorous has been made. The three semi-empirical scaling laws relate the design beam energy  $E$ , the ring radius  $R$  and the betatron tune  $\nu$ .

*The first law:*

$$\nu = \sqrt{R}$$

To apply this law, take the ring radius  $R$  in units of meters and take the square root to obtain an approximate value for the betatron tune  $\nu$ . This law applies to both electron and proton storage ring colliders.

*The second law:*

$$E = \sqrt{R}$$

This law applies only to electron rings. Again,  $R$  is expressed in meters. The result expressed in GeV is approximately equal to the beam energy.

*The third law:*

$$E = \begin{cases} R & \text{For superconducting ring} \\ R/4 & \text{For conventional ring} \end{cases}$$

This law applies to proton rings.  $R$  and  $E$  are expressed in meters and GeV, respectively.

Before discussions of these scaling laws, Figs. 7 and 8 are the experimental data confirming them. Fig. 7 is a plot of the horizontal betatron tune versus the ring radius for several electron and proton storage rings. The dashed line represents the prediction according to the first scaling law.

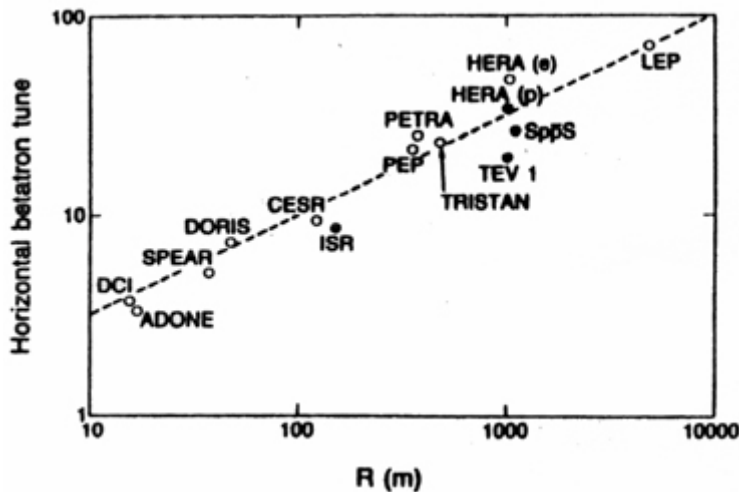


Figure 7. Data showing scaling of betatron tune with storage ring radius.

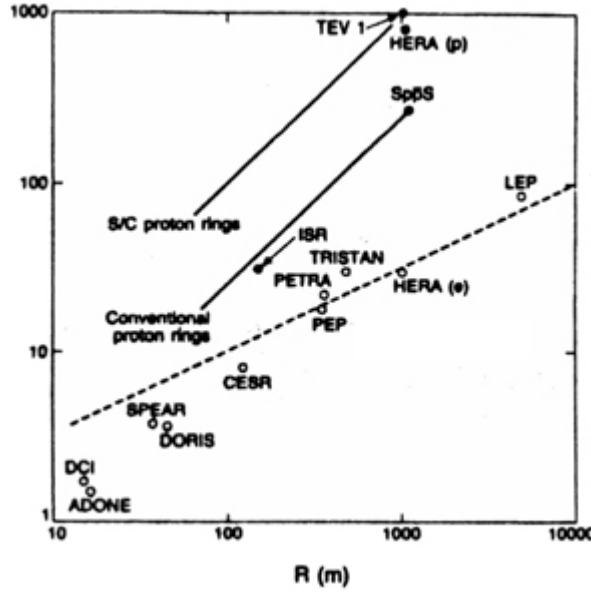


Figure 8. Data showing scaling of beam energy with storage ring radius.

Fig. 8 is a plot of the beam energy versus ring radius. The dashed line represents the second scaling law. The solid line represents the third scaling law. We see that the experimental results fit the first and the second laws quite well. As to the third law, not yet enough data points are available.

### Corollaries

There are a few corollaries of the first law. First, we learn from elementary lattice theory that the average  $\beta$ -function  $\langle\beta\rangle$  is given by  $R/v$ ; therefore applying first law gives

$$\text{corollary: } \langle\beta\rangle = \sqrt{R} \quad (16)$$

where  $\langle\beta\rangle$  is in meters. Second, the average dispersion function  $\langle\eta\rangle$  is given by  $R/v^2$ , therefore

$$\text{corollary: } \langle\eta\rangle = 1m \quad (17)$$

which says all collider rings have average dispersion function of 1 m, regardless of whether it is electron or proton ring, or its size. A third corollary applies to the momentum compaction factor  $\alpha$ . It is approximately equal to  $1/v^2$ . Therefore,

$$\text{corollary: } \alpha = 1/R \quad (18)$$

where  $R$  is in meters,  $\alpha$  is dimensionless.

Our numerical example is meant to be a superconducting proton ring. It has  $R=500$  m. Applying the corollary (16), it has an average  $\beta$ -function of 22 m. Applying the 3<sup>rd</sup> scaling law, the ring energy is 500 GeV. As a more realistic example, the electron storage ring PEP has  $R=350$  m. the scaling law predict a betatron tune of  $v=19$ , a beam energy of 19 GeV, and an average  $\beta$ -function of 19 m. These values agree quite well with the PEP data. It is also interesting to see that  $v$ ,  $E$  in GeV, and  $\langle\beta\rangle$  in meters are approximately equal for electron storage rings.

The above scaling laws obviously do not have rigorous scaling proofs. However, some understanding of storage ring designs can be obtained by studying the underlying reasons of their validity, even an approximate one. We shall begin with the proof of the third law, which is the most straightforward among the three.

### 2.2 Proof of third law

For a proton ring, the limit is the strength of the bending magnetic field. The higher the beam energy,er the ring has to be in proportion. Thus  $R \propto E$  and the third scaling law is basically proven. The difference between the conventional and the superconducting rings is due to their different bending strengths.

### 2.3 Proof of the second law

This law has two proofs, a wrong one and a right one. The wrong proof associates the scaling with a cost minimization consideration. The storage ring cost is first written as the sum of two terms,

$$\text{cost} = \text{ring cost} + \text{RF cost} \quad (19)$$

where the ring cost refers to the cost of magnets, tunnel, etc. The RF cost refer to the cost of the RF components needed to compensate for the energy loss by an electron due to synchrotron radiation. The ring cost is proportional to  $R$  and is basically independent of the beam energy. The RF cost on the other hand is proportional to the synchrotron radiation loss per turn, which is proportional to  $E^4/R$ . Thus,

$$\text{cost} = fR + g \frac{E^4}{R} \quad (20)$$

By differentiating the cost expression with respect to R for given beam energy E, the minimum cost is obtained when

$$f - g \frac{E^4}{R^2} = 0 \quad (21)$$

or

$$R \propto E^2 \quad \text{or} \quad E \propto \sqrt{R}$$

thus providing the second law.<sup>[10]</sup>

There is nothing wrong with the argument itself. In fact, this exercise leads to the important conclusion that the size and cost of large electron storage rings increases quadratically with increasing beam energy, unlike proton rings whose size and cost increase only linearly. As a consequence, super electron storage rings are unfavourable as compared with electron linac colliders.<sup>[10,11]</sup> The reason this proof is incorrect here is that it applies only when the Rf cost becomes a significant part of the total cost. This does not happen until the beam energy is of the order of 30 GeV or so. Yet the scaling law is approximately valid already around a few GeV.

A more basic reason of the second law is from the beam dynamics considerations. We mentioned before that sextupoles are inserted in the ring design to open up a finite momentum aperture for the beam. It is important that the beam energy spread does not exceed the momentum aperture so painstakingly achieved. In an electron ring, the rms energy spread is given by<sup>[1]</sup>

$$\sigma_\delta^2 = \frac{55}{64\sqrt{3}} \cdot \frac{\hbar}{m^3 c^5} \cdot \frac{E^2}{R} = 10^{-6} \frac{E[\text{GeV}]^2}{R[\text{m}]} \quad (22)$$

where h is Planck's constant, m is the electron mass, c is the speed of light.

If we use a high bending field of a conventional magnet and  $E=R/4$  as the third law predicts, for example, the energy spread will increase as beam energy increases until the momentum aperture (taken to be  $\pm 10\sigma_\delta = \pm 1\%$  in our discussion) is reached around 4 GeV or so. Beyond 4 GeV, it is necessary to impose the scaling  $E = \sqrt{R}$  thus proving the scaling law.

Inserting the scaling into Eq. (22), one obtains, for all electron collider storage rings, independent of the design energy E and the ring size,

$$\text{corollary: } \sigma_\delta = 10^{-3} \quad (23)$$

## 2.4 Proof of first law

We offer a proof for the electron case only. Basically what happens is that when  $\nu$  is chosen too large, there will have to be too many quadrupoles, which makes the ring expensive. On the other hand, if the tune is chosen too small, the beam size becomes large correspondingly until at certain point beyond which any further increase in magnet bore size will sharply drive up the magnet cost.

The rms horizontal betatron beam size  $\sigma_{x\beta}$  of an electron beam is<sup>[1]</sup>

$$\frac{\sigma_{x\beta}^2}{\beta} = 2\sigma_\delta^2 \frac{R}{\nu^3} \quad (24)$$

where  $\beta$  is the  $\beta$ -function at the point where beam size is observed. Inserting Eq. (23) for  $\sigma_\delta$  and replacing  $\beta$  by its average value  $R/\nu$ , we obtain the average rms horizontal betatron size of

$$\sigma_{x\beta} = \sqrt{2} 10^{-3} \frac{R}{\nu^2} \quad (25)$$

To restrict  $\sigma_{x\beta}$  under a realistic value,  $\nu$  has to keep pace at least as fast as  $\sqrt{R}$  as R increases. To minimize the number of quadrupole magnets,  $\nu$  is chosen to be equal to  $\sqrt{R}$ . This explains the first law for electron rings.

Substituting  $\nu = \sqrt{R}$  in Eq. (25), we obtain

$$\text{corollary: } \sigma_{x\beta} = \sqrt{2} \text{mm} \quad (26)$$

Equation (26) refers to the case in the absence of coupling between the two betatron dimensions x and y. In case of a total coupling, the betatron sizes are  $\sigma_{x\beta} = \sigma_{y\beta} = 1 \text{ mm}$ .

The total horizontal beam size is a quadratic sum of the betatron and the synchrotron sizes. In the absence of coupling, its value is given by

$$\sigma_{x,tot} = \sqrt{\sigma_{x\beta}^2 + \eta^2 \sigma_\delta^2} = \sqrt{3} \text{mm} \quad (27)$$

where we have used the property that  $\eta = 1 \text{ m}$  and  $\sigma_\delta = 10^{-3}$ .

Equations (26) and (27) apply to all electron rings independent of ring size and design energy.

\* \* \*

#### REFERENCES

- [1] M. Sands, SLAC-121 (1970).
- [2] W. Weng, this summer school (SSC-45).
- [3] K. Robinson and G. Voss, CEA report CEAL-TM-149 (1965), unpublished.
- [4] P.L. Morton and J.R. Rees, IEEE Trans. Nucl. Sci., NS-14, 630 (1967).
- [5] L. Smith, SLAC note PEP-20 (1972), unpublished.
- [6] G. Fisher, SLAC note SPEAR-154 (1972), unpublished.
- [7] C. Pellegrini, Nuovo Cimento 64, 477 (1969).
- [8] M. Sands, SLAC-TN-69-B (1969).
- [9] K.L. Brown and R.V. Servranckx, 1983 Accelerator Summer School, BNL/Stony Brook, AIP Conf. Proc. 127.
- [10] B. Richter, Nucl. Inst. Meth., 136, 47 (1976).
- [11] M. Tigner, Nuovo Cimento, 37, 1228 (1965).